The design and evaluation of a personalized 3D-printed hand brace with pressure sensors for enhanced functionality and continuous feedback monitoring

BM51035: MSc-Thesis

Argyropoulos Athanasios

TU Delft

The design and evaluation of a personalized 3D-printed hand brace with pressure sensors for enhanced functionality and continuous feedback monitoring

By

A. Argyropoulos

To obtain the degree of Master of Science
at the Delft University of Technology,
to be defended publicly on November 28, 2023

Student number:	5390117	
Project duration:	11/2022 – 11/2023	
Supervisor:	Dr. Ir. N. Tümer	TU Delft
Thesis committee:	Dr. Ir. N. Tümer	TU Delft
	Dr. Ir. G. Smit	TU Delft
	Prof. Dr. M.J Mirzaali	TU Delft

TU Delft

Preface

This thesis represents the final step towards completing a journey that commenced 1 year ago. During this time, I had the honor of collaborating with exceptionally intellectual individuals, whose assistance was crucial in overcoming obstacles and challenges that emerged during the duration of this project and ultimately contributed to its successful completion.

Prior to anything else, I would like to express my gratitude to my main supervisor, Dr. Ir. Nazli Tümer for her scientific guidance and constructive criticism, and belief in me throughout the completion of this thesis.

I would like to thank the PhD candidates from Biomaterials and Tissue Biomechanics department for their willingness to assist me with the fabrication process of this thesis.

Sincere thanks to my friends, Chrysovaladis, Xristos, Stavros and Odysseas during my master studies. The development and completion of this thesis wouldn't have been possible without their support and questions.

Finally, deep-hearted thanks to my parents, Olympia and Dimitris and my sister, Evangelia for their love and belief in me.

Argyropoulos Athanasios
Delft, November 2023

Contents

NOMENCLATURE VI

LIST OF FIGURES VII

LIST OF TABLES IX

ABSTRACT 1

INTRODUCTION 2

1.1 BACKGROUND 2
1.1.1 FACTORS INFLUENCING PATIENT NONADHERENCE 3
1.1.2 WEARABLE ELECTRONICS IN PROSTHETICS FIELD 3
1.2 STUDY GOAL 4

METHODS 5

2.1 STUDY OVERVIEW 5
2.1.1 DESIGN CRITERIA 5
2.2 DESIGN PROCESS AND MANUFACTURING 6
2.2.2 CLOSURE MECHANISM 9
2.3 ELECTRONICS 9
2.3.1 SENSORS 9
2.3.2 MICROCONTROLLER 12
2.3.3 ARDUINO CASE AND INNER SURFACE 13
2.4 FINITE ELEMENT ANALYSIS 14
2.4.1 GEOMETRY DEFINITION – VALIDATION OF THE FEM 14
2.4.2 DESIGN PROCEDURE 14
2.4.3 MATERIAL ASSIGNMENT 15
2.4.4 MESH GENERATION 15
2.4.5 INTERACTIONS 16
2.4.6 BOUNDARY AND LOAD CONDITIONS 17
2.5 EXPERIMENT 17
2.6 POST-PROCESSING – DASHBOARD DESIGN 19

RESULTS 21

3.1 ASSEMBLY OVERVIEW 21
3.1.1 3D-PRINTED HAND BRACE 21
3.1.2 VALIDATION PROCEDURE - 3D BONE GEOMETRIES 22

3.2 POST-PROCESSING 23
3.2.2 FINITE ELEMENT ANALYSIS 23
3.2.3 COMPARISON BETWEEN FEM - EXPERIMENTS 24
3.2.4 DASHBOARD 27

DISCUSSION 28

CONCLUSION 32

REFERENCES 33

APPENDIX A 38

ARDUINO CODE 38

APPENDIX B 43

ASSEMBLY 43

Nomenclature

Abbreviations

ABBREVIATION	DEFINITION
AM	Additive Manufacturing
CT	Computed Tomography
CAD	Computer-Aided Design
CMC	Carpometacarpal
FE	Finite Element
FEA	Finite Element Analysis
FEM	Finite Element Model
FSR	Force Sensitive Range
MCP	Metacarpophalangeal
MRI	Magnetic Resonance Imaging
RP	Reference Point
TPU	Thermoplastic Polyurethane
EXP	Experiment

List of Figures

Figure 1. Schematic of the a) human's forearm, b) forearm with removing background, c) applying mask in agisoft to select points of interest, d) forearm model in tie points, e) the points around the forearm represent the noise. 7
Figure 2. a) Digital forearm model in agisoft b) forearm model with cut edges in meshmixer c) Single Surface of Hand brace in meshmixer d) Render of final hand brace model e) 3D-printed Hand brace. 7
Figure 3. a) 3D view of the hand brace in CURA, b) Infill inside the hand brace and c) Infill pattern of 3D cross. 8
Figure 4. a) Final design of the 3D-printed straps, b) watch strap with PLA bolts for closure and a case for the microcontroller and c) 3D-printed straps with magnets. 9
Figure 5. Schematic of the a) circuit of an FSR and b) Resistance-Mass calibration curve [51]. 10
Figure 6. Calibration curve of the FSR model 402 with curve-fitting (R^2=0,9983). 11
Figure 7. a) Render of the front view of the hand brace with embedded FSR sensors. b) Design and characterization of FSR® Model 402 Short Tail [51]. 12
Figure 8. a) Render of the front view of the 3D-printed hand brace, b) Render of the side view of the 3D-printed hand brace c) Real representation of the Arduino inside the case at the top of the 3D-printed hand brace. 13
Figure 9. a) Placing wires and FSRs inside the 3D-printed hand brace, b) 3D-printed inner surface c) 3D-printed inner surface inside the 3D-printed hand brace to cover the cables. 13
Figure 10. Render of the front view of the 3D bone structures in blender a) to f) simplified process of hand and arm, g) connected simplified arm and hand models to design the simplified skin and h) assembly of the arm, hand, and skin. 15
Figure 11. a) Defined interactions in the 3D-printed hand brace model, b) UJOINT connecting both bones, representing wrist movements via the hand reference points. 16
Figure 12. a and b) The movements of wrist: extension and flexion [62], c) Boundary conditions applied to the 3D-printed hand brace and the bone. 17
Figure 13. The positions of the six FSRs models inside a) the brace in Abaqus, b) inside the 3D-printed hand brace. 18
Figure 14. a) Pressure values from the six sensors as outlined in dashboard, as well as the equations of how to convert force to pressure, b) the 3D-printed hand brace that is worn by a participant and an object that was used to carry the weights for the experiment. 19
Figure 15. a) Overview of the 3D-printed hand brace b) Overview of the 3D-printed hand brace on the participant's hand. 22
Figure 16. Render of the complex and simplified 3D bone geometries and the maximum Stress values in Abaqus during wrist movement. 22
Figure 17. The percentage of immobilization under extension (top) and flexion (bottom) and the distribution of the von Mises stress (MPa) of the deformed 3D-printed hand brace for both wrist movements. 23
Figure 18. Pressure distribution (MPa) of the deformed 3D-printed hand brace for both wrist movements a) extension and b) flexion. 23
Figure 19. Comparison of the experiment and FEM, line plots of the wrist movements, a) extension and b) flexion 26
Figure 20. Overview of the Website UI in Arduino IOT cloud. a) Progress of wearing duration every 1 hour about the tightness of the 3D-printed hand brace. b – c) daily reminders of the treatment. d) Display the tightness of the brace on change. e) Monitor the time left. f) Display all the FSR pressure values on change. 27

Figure 21. Representation of all the parts that consists in the 3D-printed hand brace. A) 3D-printed hand brace, B) 3D-printed Arduino case, C) Arduino MKR 1010, D) FSRs, E) Cable Connector, F) 3D-printed inner surface, G) 3D-printed straps. 43

List of Tables

Table 1. Print Settings Parameters for 3D-Printed Hand Brace using TPU 95A in CURA Ultimaker version 5.3.0. 8
Table 2. Mechanical properties of the parts considered in the FEA. 15
Table 3. Printing time [min] and material weight [g] for all parts 21
Table 4. Pressure values from FRSs during extension wrist movement. EXP represents experiments. 24
Table 5. Pressure values from FRSs during flexion wrist movement. EXP represents experiments. 25

Abstract

Background: In the field of orthoses for the treatment of forearm injuries, there is a growing clinical demand for more precise and individualized health monitoring technologies. The integration of additive manufacturing techniques with wearable electronics has gained significant interest in this field, emerging as a prominent treatment option that aims to address this demand and gradually replacing conventional rehabilitation approaches. While the medical benefits of orthoses are well-established, a significant challenge persists in ensuring patient adherence to suggested usage guidelines.

Objectives: This thesis aims to develop a systematic workflow for providing personalized feedback to patients, with the objective of 1) improving their functional recovery throughout the rehabilitation process, and 2) facilitating patient adherence to their prescribed treatment plan.

Methods: A general workflow for the utilization of wearable electronics inside an orthotic device is proposed. This workflow accounts for the physical interactions between the user and the orthotic device itself. Particularly, an elastomer material was used to fabricate the hand brace with six commercially available force-sensitive sensors and a microcontroller for data processing and integration, into the proposed workflow. Each element of this workflow is discussed with respect to the role that it plays in the treatment of a forearm injury, along with how the data of each sensor can be used as inputs to the designed platform that aims to monitor the patient compliance to the treatment plan. Through an accessible web interface, users can conveniently track their treatment progress, receive real-time feedback on brace usage and monitor wear duration. Concurrently, clinicians can gain access to valuable monitoring capabilities, facilitating data-informed adjustments for personalized care. To validate the effectiveness of the designed 3D-printed hand brace, finite element simulations and experiments were conducted to evaluate the immobilization of the hand brace and study pressure distribution, by applying the brace on a participant's hand.

Results: Simulation results were compared to those of experiments and demonstrate positive outcomes, affirming the brace's ability to provide support for forearm fractures with 85% immobilization for the hand rotation under wrist movements. The maximum average pressure values observed during experiments were less than 0.3 MPa for wrist flexion and 0.2 MPa for wrist extension.

Conclusion: The proposed method outlines a multistep process that lays the foundation for future advancements in orthopedic brace design and personalized healthcare. It offers an objective means of monitoring patient adherence to forearm treatment methods and allows a trained healthcare worker to 3D-print a brace based on the initial medical diagnosis and subsequently modify the treatment method considering the data captured via platform during the user's daily activities.

Key words: forearm fractures, orthosis adherence, 3D printing, hand brace, wearable electronics, pressure sensors

1

Introduction

This chapter presents a comprehensive review of forearm fractures and their treatment approaches, with a particular emphasis on the important issue of patient compliance with wrist rehabilitation guidelines. The following sections delve into two key aspects of this complex landscape: the factors that affect patient adherence to orthosis and the impact of incorporating wearable electronics in prosthetics. Finally, the aim of this thesis project is stated.

1.1 Background

Forearm and wrist fractures are common injuries, often resulting from trauma, such as falls, sports injuries, and accidents [1]-[12]. The treatment of these fractures varies depending on factors like the severity and location of the injury while the primary goal of the treatment remains consistent: to realign and stabilize the fractured bones, and thus facilitating proper healing while minimizing long-term adverse consequences [1], [13]-[19]. In many cases, casting or splinting may be sufficient to immobilize the affected area and promote bone union, especially for stable fractures that do not require surgical intervention [8],[9],[16],[19]. A prior literature review, conducted by the same author as this thesis, explored various treatment methods for wrist fractures. This review considered factors like patient satisfaction, comfort, and pain. The findings demonstrated generally higher patient satisfaction with modern approaches, including the utilization of 3D-printed orthoses [20]-[32]. Accordingly, this thesis is focused on 3D printing as a multistep manufacturing technique to design and develop hand braces.

In contemporary medical practice, 3D-printed orthoses, particularly hand braces, are commonly prescribed for the treatment of distal radius fractures, carpal tunnel syndrome and osteoarthritis (OA) [8]. These braces also used in the treatment of acute and chronic orthopaedic conditions. Patients are often prescribed such orthoses with recommendations to use them consistently over extended periods, ranging from a few weeks for tendon injuries to potentially several years for those recovering from strokes [8]. Despite the medical benefits of orthoses are well-established, a significant challenge persists in ensuring patient adherence to prescribed usage guidelines [33].

1.1.1 Factors Influencing Patient Nonadherence

Patient adherence presents a distinctive challenge, particularly among patients undergoing upper extremity rehabilitation. Extensive research underscores the pivotal role of adherence in improving outcomes for upper extremity conditions [33]-[36]. Nonadherence to orthoses results in reduced treatment efficacy, heightened disability risks, and compromised treatment evaluation, especially in adults recovering from acute upper limb injuries [37]. The rates of orthosis adherence in hand treatment exhibit significant variation, ranging from 17% to 92%, mostly due to the use of diverse adherence standards [38].

To be more precise, treatment adherence as defined by the World Health Organization's (WHO), refers to the degree to which an individual's behavior conforms to the recommended guidelines provided by a healthcare professional [35],[36]. In a therapeutic context, precise adherence documentation is crucial for clinicians to assess treatment efficacy. In a research context, it is essential to measure the degree of adherence to a particular intervention in order to appropriately assess its success (immobilization percentage) and comprehend its impact on clinical practice [33],[37].

Presently, assessing patient adherence to orthosis mostly relies on subjective measures, such as patient diaries, questionnaires, and interviews [33]. However, these records may include subjectivity and are prone to memory biases, particularly when evaluating adherence many weeks or months after the prescription. In addition, it should be noted that these assessments have the potential to unintentionally impact on patient behavior [39]. To overcome these constraints and facilitate the development and use of orthosis designs that are more successful, it is crucial to establish a reliable method for monitoring participants' adherence to wearing the orthosis as prescribed. The task of accurately and reliably assessing adherence poses more challenges when therapies require patient cooperation and supervision outside clinical settings [33],[35]. In response to these challenges and the need for objective measurement of the patient’s comfort levels, extensive research [33]-[35],[38] has explored the pressure distribution under the orthosis and the compliance monitoring, notably through wearable electronics.

1.1.2 Wearable electronics in prosthetics field

In prosthetics field, the integration of wearable electronics represents a recent technological advancement that has garnered attention, particularly concerning factors influencing patient compliance and the capacity for sensor data measurement. This technology has enabled the assessment of wear duration through strap tension analysis, integration of a load-monitoring system, and the prevalent utilization of pressure and temperature sensors embedded within braces [40],[42].

In the literature, there are many researchers that investigate the use of wearable electronics in prosthetics field. A study conducted by Akiyama et al. (2016) used pressure sensors integrated into the cuff of a lower-limb active orthosis to monitor contact force on the thigh. The purpose of this approach was to minimize the risk of skin injuries [43]. In their study, Dzedzickis et al. (2020) included soft sensor strips that were incorporated into a lower limb prosthesis to assess comfort levels. This was achieved by using socket pressure mapping techniques during both walking and standing activities [44]. In a separate investigation, a pressure sensor mat was used to assess the contact pressure experienced by individuals wearing a wrist orthosis for the treatment of carpal tunnel syndrome. The pressure measurements were taken at various wrist

angles [45],[46]. Further applications involved monitoring contact pressure under scoliosis orthoses using air pressure sensors and even the development of personalized 3D-printed footwear with embedded sensors [47]-[50].

These innovations enable remote healthcare monitoring, allowing patients to remain at home, reducing the burden on healthcare facilities. However, the existing literature lacks objective data on the frequency and timing of prosthesis use. Hence, this thesis focus is on providing feedback to patient by continuously following them and creating a simplified platform to inform the orthotic user. To achieve this, integration of readily available and replaceable piezoelectric sensors is pursued. Additionally, the utilization of an intuitive web and app interface for data monitoring and analysis is proposed, presenting a potential solution to the aforementioned challenges.

1.2 Study Goal

This thesis's primary objective is to develop a personalized hand brace with embedded pressure sensors, enabling continuous monitoring and providing the user with feedback. Furthermore, the brace should provide support for immobilizing the wrist in cases of fractures or injuries. To gain insights into the contact region under a tailored hand prothesis and the immobilization potential of the prosthesis, a Finite Element Model (FEM) is constructed. Following this, an experiment is set to validate the simulations.

This thesis aims to develop a systematic workflow for providing personalized feedback to patients, with the objective of 1) improving their functional recovery throughout the rehabilitation process, 2) facilitating patient adherence to their prescribed treatment plan.

2

Methods

In this chapter, the methodology of the thesis is comprehensively outlined. The design overview and the design criteria are explained in 2.1. After the design and manufacturing process, finite element analysis (FEA) is conducted to explore the functional performance of the 3D-printed hand brace. In the next section, to gain insight into the pressure distribution at the contact area under a tailored hand and 3D-printed hand brace, FEM and experiments are constructed. The main goal of the experiment is to validate the computational analysis.

2.1 Study Overview

The design and development of the 3D-pritned hand brace encompasses a thorough integration of digital and manufacturing processes in a methodical manner. The process starts with the careful acquisition of comprehensive forearm characteristics via the use of a smartphone. Subsequently, a series of pictures is examined and converted into a three-dimensional depiction of the forearm. Following the first stages of the digital refining, further steps include the reduction of noise and the alignment with the human forearm, ultimately leading to an enhanced digital depiction of the forearm model. Regarding, the hand brace design, it relies on this digital forearm model as its fundamental base, which entails the selection of the outer surfaces of the forearm and then, the modification of its final design. Concurrently, the hand and arm bone geometries that have been obtained from an anonymized CT scan, undergo simplified processing to reduce the computational load, with a particular focus on aligning them with the skin of the forearm model. The next phases include the development of meshes, assigning materials, and applying forces using advanced software platforms to conduct finite element simulations. In the second phase of the methodology, the integration of piezoelectric sensors and a microprocessor inside the hand brace enables the real-time acquisition of data. The utilization of simulation data, and implementation of user-friendly interfaces, result in the workflow of this thesis, ultimately leading to an objective way to monitor patient adherence to prescribed treatment.

2.1.1 Design Criteria

Before getting into the major design and manufacturing techniques, it is essential to evaluate a multitude of factors that must be thoroughly addressed in order to successfully build a 3D-printed hand brace. The design process was notably influenced by the need to accommodate the unique demands of the orthosis, which included careful consideration on materials, electrical components, and the capacity to assess the patient's adherence to the treatment plan. Particularly, the selection of materials must exhibit mechanical features, including biocompatibility, flexibility, and nontoxicity, to provide the patient with maximum support,

comfort, safety and an aesthetically pleasing appearance [53]. Additionally, the electronic components, including the piezoelectric sensors and microcontroller, were strategically arranged within the hand brace to ensure a non-intrusive design that can be comfortably worn by patients in research settings. Furthermore, the 3D-printed hand brace had to be readily adjustable and washable, facilitating for regular maintenance and patient-specific adaptation. These design criteria were condensed into a comprehensive list to direct the creation of the customized hand brace.

The above considerations have been summarized in the following list:

- The hand brace must be able to fit accurately on the patient's hand
- The hand brace must be able to continuous monitoring so that patient adherence to the treatment method can be followed

- The manufactured material must have the following specifications:
    - Biocompatible
    - Flexible
    - Nontoxic
    - Long lasting (2 to 6 weeks)
    - Provide an aesthetically pleasing appearance

- The electronics of the hand brace must meet the following criteria:
    - The piezoelectric sensors must be in touch with the patient's skin
    - The microcontroller and the cables must be covered
    - The sensors must be thin to fit under the hand brace
    - The sensors must be able to gather data about the pressure distribution to access the comfort levels of the brace

- The hand brace must be easily adjustable and cleanable
- The electronics must be inside a detachable case to facilitate repairability

2.2 Design Process and Manufacturing

2.2.1 Hand Brace

The design procedure of developing a 3D-printed hand brace involved a well-planned and multistep approach, emphasizing the importance of patient's precise and comfortable fit. The complex process started with the digitalization of the human forearm, using advanced post-processing techniques. The dataset consists of multiple images of the forearm, which have been meticulously captured from various viewpoints using a smartphone (**Figure 1** a). The collection of photos was thereafter submitted to a thorough processing procedure using Metashape Agisoft including processes like removing background (**Figure 1** b), applying masks to select only the points of interest (**Figure 1** c), deleting the points that were outside the main forearm model (**Figure 1** d, e). The software not only enables the importing of pictures but also does extensive data refining, effectively removing noise. The result of this curating process was a flawless digital representation of the human forearm.

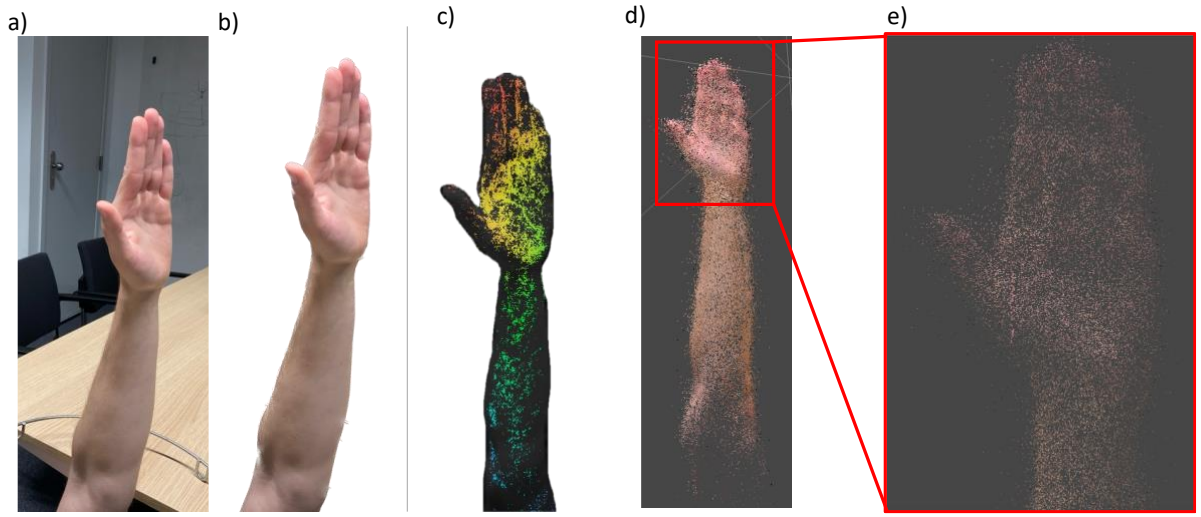

Figure 1. Schematic of the a) human's forearm, b) forearm with removing background, c) applying mask in Agisoft to select points of interest, d) forearm model in tie points, e) the points around the forearm represent the noise.

The next step involved a scaling process between the digital model and the physical forearm. In MeshLab, the forearm model was scaled based on the dimensions of the participant's forearm, due to the fact that the scanning process was done by a smartphone and not by an advanced scanning technique (**Figure 2** a). In the software Blender, the surfaces were flawlessly refined by deleting any surface points irrelevant with the forearm model (**Figure 2** b). After achieving the desired result in the forearm model, it proceeded to Meshmixer. More specifically, this stage involved the careful selection of the outer surfaces of the forearm model that consist of the hand brace and accurate cutting of the edges of the forearm model, all precisely customized to guarantee adherence to the forearm's shape (**Figure 2** c). The last step was modifying the thickness of the brace, which may be easily achieved using the offset command (**Figure 2** d). The final design of the hand brace model was completed as shown in **Figure 2** e.

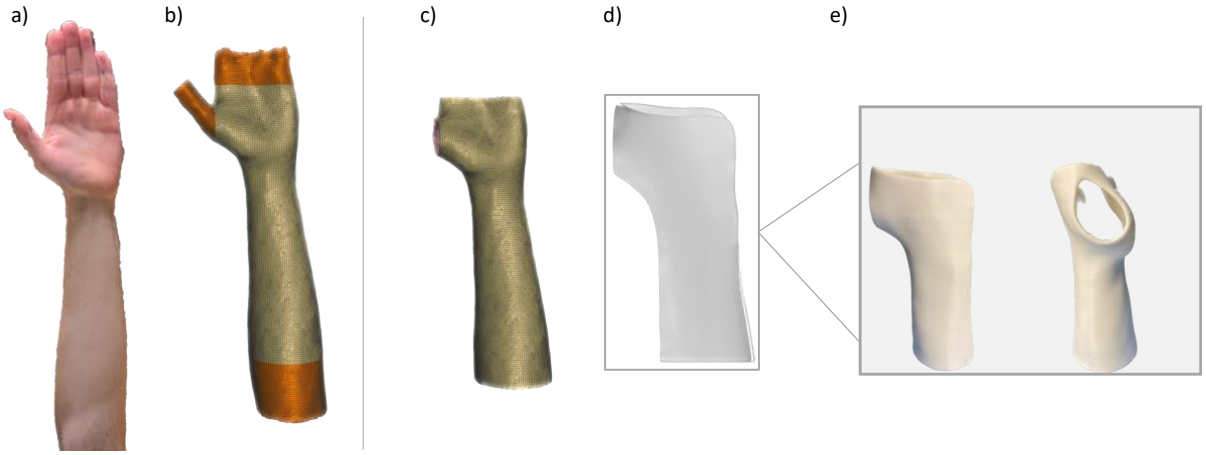

Figure 2. a) Digital forearm model in Agisoft b) forearm model with cut edges in meshmixer c) Single Surface of Hand brace in meshmixer d) Render of final hand brace model e) 3D-printed Hand brace.

After finalizing the design of the hand brace, the 3D printing process was initiated. The digital model of the hand brace was imported into CURA (Ultimaker Cura, version 5.3.0), a slicing software for 3D printers. In CURA, optimal printing parameters, such as print speed and temperature, layer height, and infill density were set to ensure a printable model. To evaluate the brace's effectiveness on the participant's hand, an initial prototype was 3D printed using

ABS filament. Feedback from the participant and lab technicians guided necessary modifications to the design. The final version of the hand brace was printed using thermoplastic polyurethane (TPU) 95A filament on an Ultimaker S2+ Connect which provided the necessary flexibility for a wearable orthotic device.

Further exploring the manufacturing process of the 3D-printed hand brace, it was fabricated using different infill densities. The selection of infill density and infill pattern was intended to accomplish varying degrees of rigidity in various regions of the brace to enhance comfort levels and support, as well as provide a solid base in the wrist region where the sensors would be placed. In CURA, this was achieved by selecting a blocker and define it as "mesh only" and align it with the hand brace (**Figure 3**). The position of the hand brace at the horizontal axis was done for two reasons. First, to allow less support and second, as TPU95A was prone to oozing, it was recommended by the Ultimaker to design and position the part such that limited travels are needed. All the printing parameters are shown in **Table 1**.

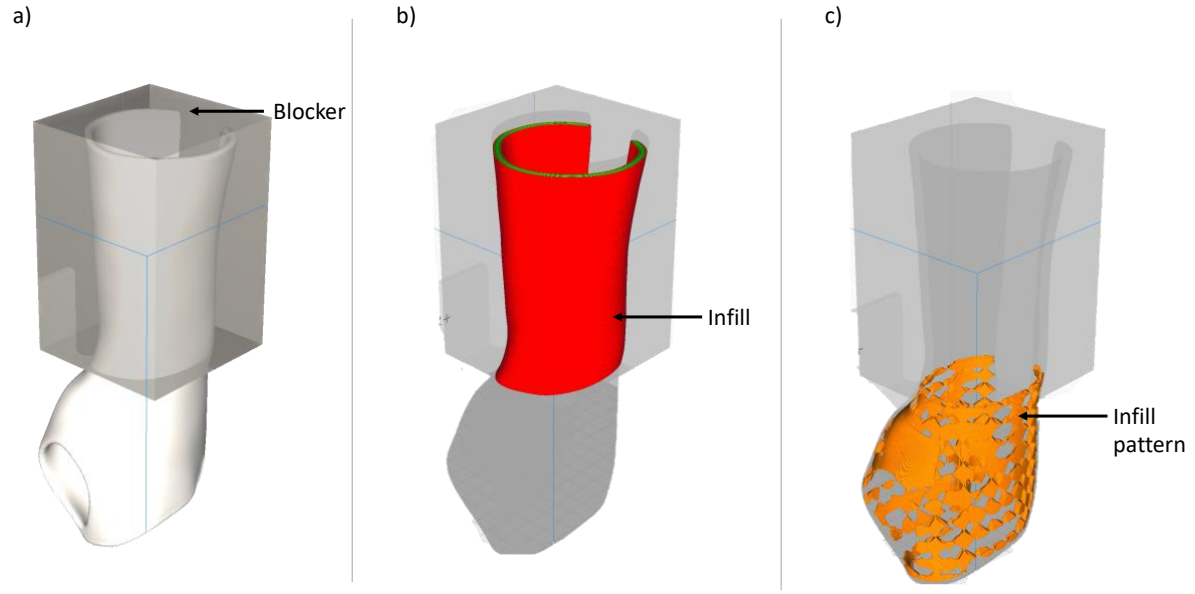

Figure 3. a) 3D view of the hand brace in CURA, b) Infill inside the hand brace and c) Infill pattern of 3D cross.

Table 1. Print Settings Parameters for 3D-Printed Hand Brace using TPU 95A in CURA Ultimaker version 5.3.0.

Printing parameters		**Nozzle**		**Plate**		**Support Blocker**	
Layer height	0.1mm	Diameter	0.4 mm	Temperature	30°C	Mesh type	Normal
Wall thickness	1.6 mm	Temperature	225°C	Adhesion Type	Brim	Wall Thickness	0.8mm
Top thickness	2.0 mm	Print Speed	20.0 mm/s	Brim Line Count	5.0 mm	Infill Density	12%
Infill	0%	Enable Retraction	On	Cooling	Of	Infill Pattern	Cross 3D
Support Pattern	Zig Zag	Retraction Speed	20.0 mm/s				
Support Density	12%	Retraction Distance	2.0 mm				

2.2.2 Closure Mechanism

Regarding the closure mechanism, different designs were made, and approaches were taken, including standard straps (**Figure 4** a), a watch strap with PLA bolts for closure (**Figure 4** b), and straps with embedded magnets (**Figure 4** c). The final design had a flexible setup with a dorsal-ulnar opening and surrounding straps that can be adjusted to meet variations in forearm. TPU filament was selected to 3D print the straps with 1mm thickness in CURA. Self-adhesive Velcro straps were placed on the straps to allow an effortless tightening approach, with an easy releasing, and replacement as necessary. This mechanism ensured that the patient had a secure and reliable fit and a comfortable wearing experience. In this way, the 3D- printed hand brace had the capability to be detachable, depending on the specific requirements of the patient as decided by the attending clinician (**Figure 4**).

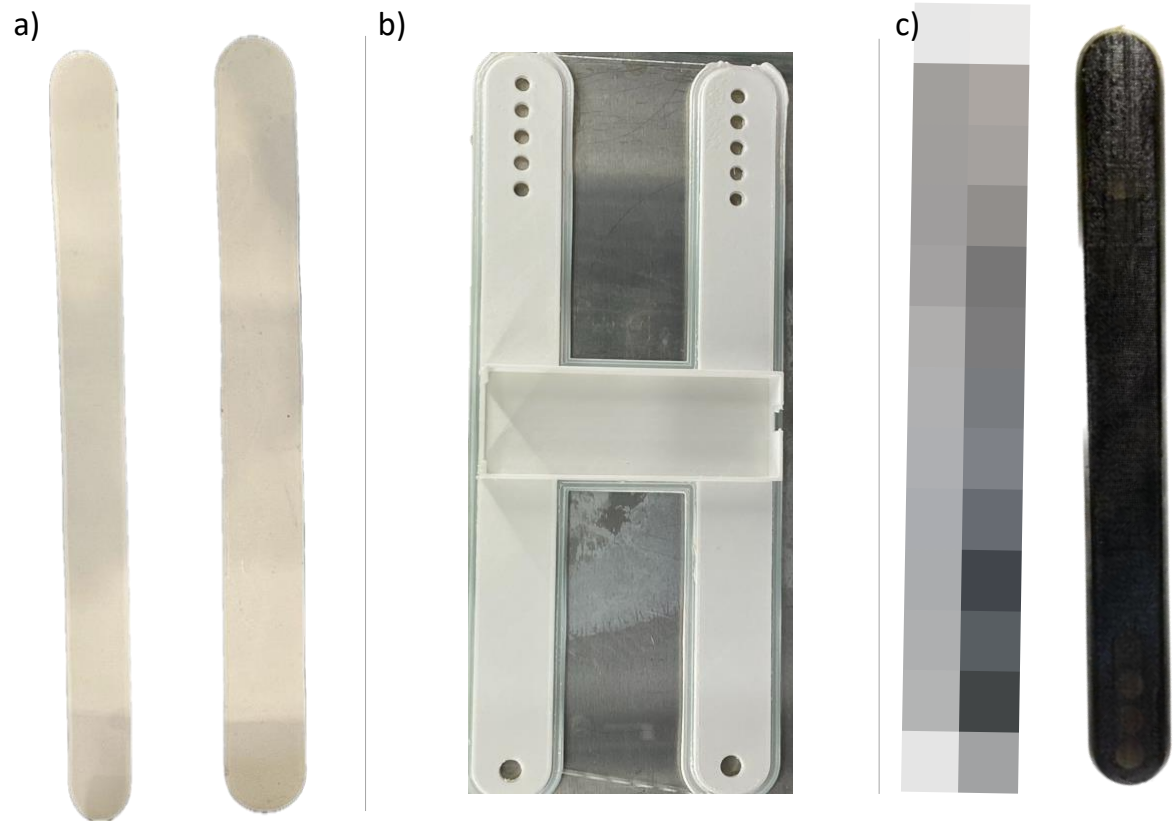

Figure 4. a) Final design of the 3D-printed straps, b) watch strap with PLA bolts for closure and a case for the microcontroller and c) 3D-printed straps with magnets.

2.3 Electronics

2.3.1 Sensors

The next step of the workflow was the selection and incorporation of piezoelectric sensors, particularly, force-sensitive resistor (FSR), into the design to measure physical pressure between the hand brace and the skin. More specifically, an FSR consists of a conductive polymer material that is placed between two layers of electrodes. This configuration enables the resistor to exhibit electrical responsiveness to variations in stress and strain. The main role of an FSR is to document data regarding whether the sensor has been pressed, and how much pressure is applied on its actuation area, while its actuation force is 0.2N and the force

sensitivity range is 0.2N – 20N [51]. FSRs are often used in ergonomic or rehabilitative contexts, where they are subjected to pressure exerted by human contact and their resulting reaction is measured or converted into another kind of output, like pressure. They are highly helpful for human engagement due to their thin design, cost-effective fabrication, and flexible geometric formations. In the configuration shown, the output voltage increases with increasing mass (**Figure 5**).

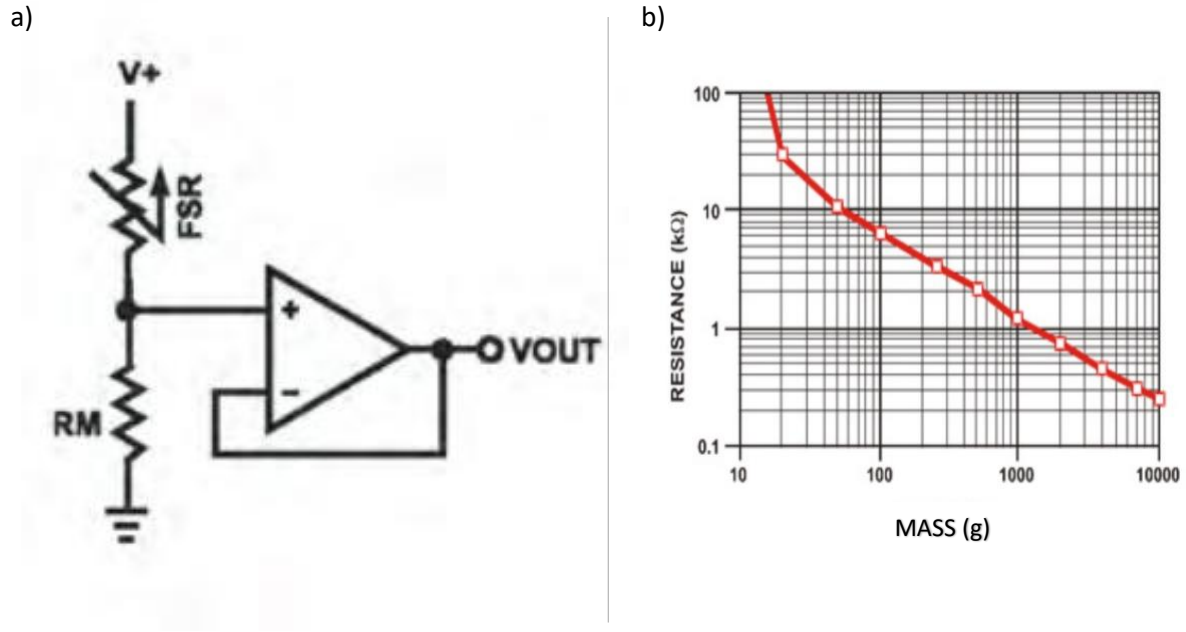

Figure 5. Schematic of the a) circuit of an FSR and b) Resistance-Mass calibration curve [51].

Concurrently, the use of an Arduino board is proposed for the purpose of acquiring and interpreting the analog signals emitted by the FSR inside a voltage divider arrangement (**Figure 5** a). This configuration allows for an estimation of the force exerted on the FSR by using the calibration curve of the sensor (**Figure 5** b). The focus is placed on using the calibration curve provided by the manufacturer, supplemented with an extra calibration check. This procedure guarantees that the sensor is operating in accordance with the anticipated behavior, and any necessary adjustments may be implemented in response to sensor drift [51],[52]. In order to achieve the highest level of accuracy in this study that need accurate force measurements, it becomes imperative to conduct component calibration. The use of calibration is recommended in situations when a higher level of accuracy is desired and curve fitting is considered to be the most comprehensive approach [51],[52]. A parametric curve fitting procedure is used to determine the nominal curve of FSRs [49]-[52].

In this thesis, the FSR was calibrated using the manufacturer resistance-mass curve (**Figure 5** b) by using the curve-fitting methodology. The resulted curve was shown in **Figure 6** with power fit and R^2=0,99 and the power relationship can be written as follows:

$$y = 26.974.849,5799x^{-1,2968} \quad (1)$$

where y is a known mass value, and x is the instantaneous resistance value generated by the Arduino and the coefficients a, b found in this thesis were: a = -1,2968, b = 26974849.

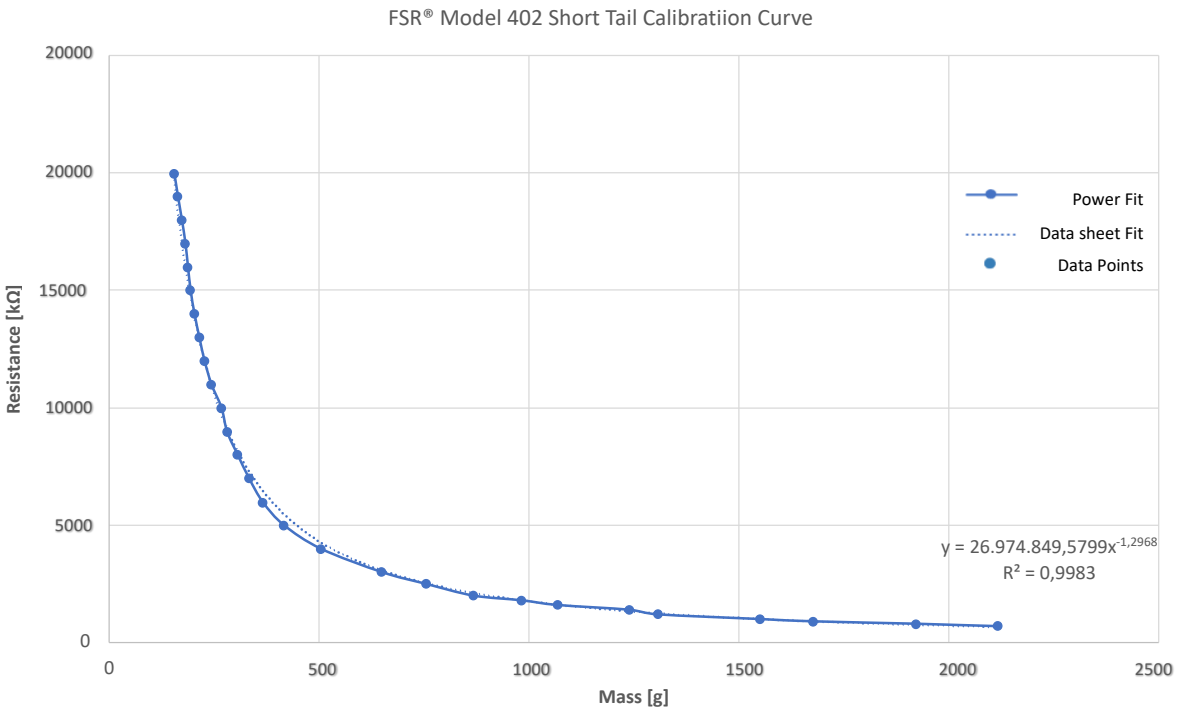

Figure 6. Calibration curve of the FSR model 402 with curve-fitting (R^2=0,9983).

Once the calibration of the FSRs was completed, six FSR® Model 402 Short Tail sensors were selected based on their specific form and size to be used for the purposes of this study [51]. These FSRs were used to examine the pressure distribution around the wrist area and the equation 2 was used to read the output voltage:

$$Vout = Vcc\frac{R_M}{R_M + R_{FSR}} \quad (2)$$

where the variable resistance of the FSR was labeled as R_{FSR}, the known resistance value was labeled as R_M,Vout was the Voltage output and Vcc (V+) was the power supply. More information regarding the Arduino code and all the equations that were used to read the FSRs and convert the output voltage to pressure were presented in Appendix A.

Regarding the CAD model of the FSR, it was created using Blender. The model was appropriately aligned with the geometry of the hand brace as seen in **Figure 7** a. Furthermore, due to the surface complexity of human wrist, small flat plates of 1mm thickness at the same size with the FSR were 3D printed using PLA in Ultimaker S2+ with the default printing settings for PLA. In the next step, they were attached in the posterior side of the FSRs in order to improve the accuracy of the measurements due to the complexity of the wrist curves.

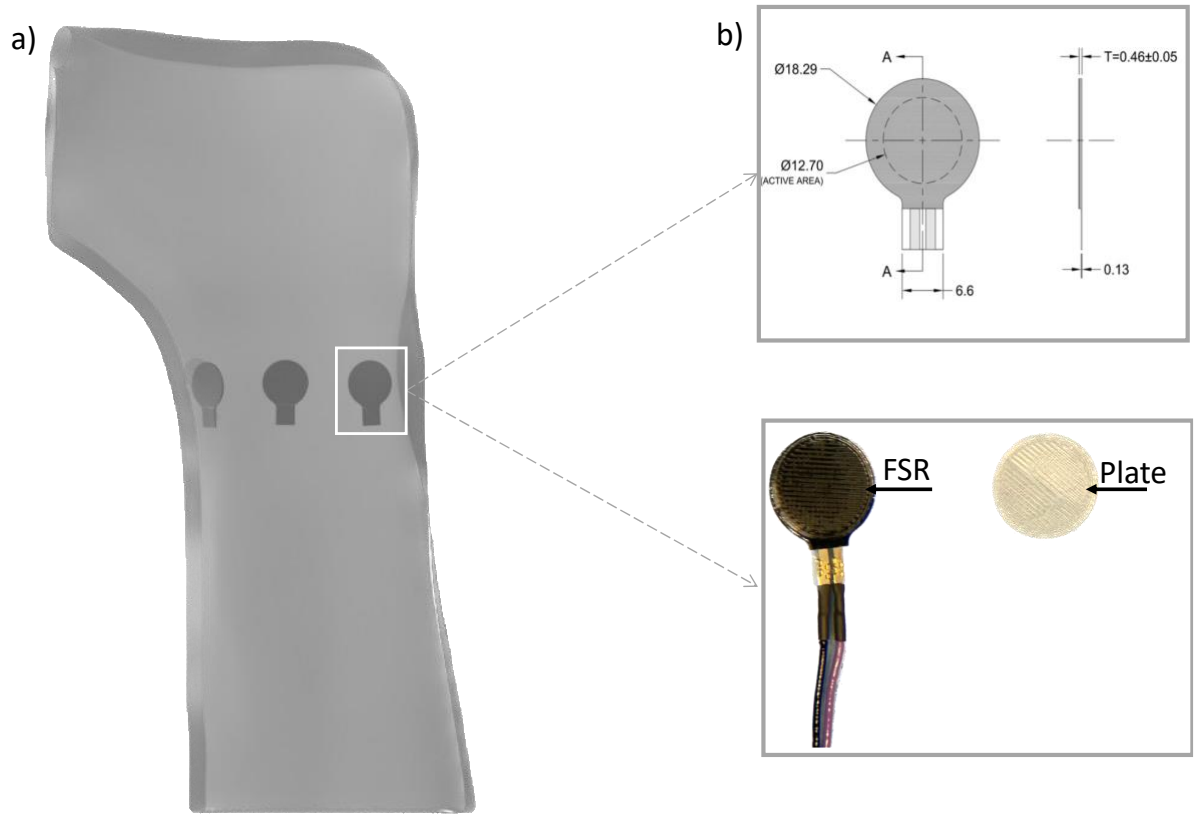

Figure 7. a) Render of the front view of the hand brace with embedded FSR sensors. b) Design and characterization of FSR® Model 402 Short Tail [51].

2.3.2 Microcontroller

To monitor the output of the FSRs and to facilitate the microcontroller's integration into the system, an Arduino MKR 1010 microcontroller was utilized and placed with cables and resistors on a custom PCB (Printed Circuit Board). This PCB design offered a space-saving and effective means of connecting the microcontroller to the FSRs and other electronic components (**Figure 8** a, b). Regarding the selection of the known resistor value, to get enhanced sensitivity at greater forcing, it is advisable to choose for a lower known resistance value. Conversely, for improved sensitivity at lower forcing, selecting a higher known resistance value is recommended. Therefore, six resistors with a resistance of 4.7 kilohms were used for the purpose of this thesis.

Additionally, two pairs of Micro JST PH 2.0 6-pin grid size 2mm connectors (male and female) were utilized to facilitate the connection and disconnection of the FSRs with the Arduino microcontroller (**Figure 8** c). This connector system streamlined the wiring and guaranteed a secure connection between the sensors and the microcontroller. The use of connectors also allowed the 3D-printed hand brace to be utilized without the sensors, accommodating varying monitoring and treatment needs. Finally, the Arduino microcontroller was connected to a laptop by using its onboard USB connector. An overview of all the electronics parts that were bought for this study are shown in **Figure 8**.

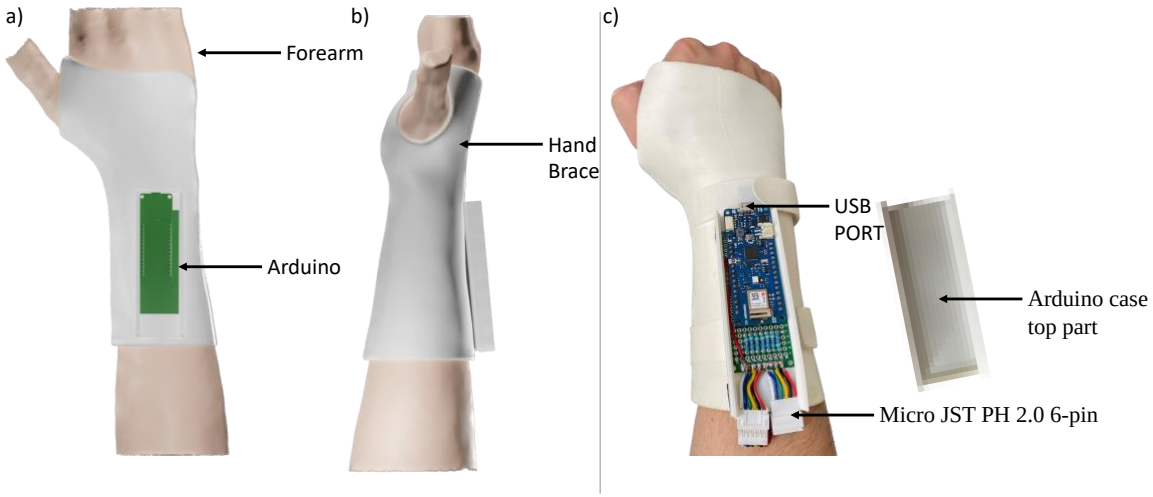

Figure 8. a) Render of the front view of the 3D-printed hand brace, b) Render of the side view of the 3D-printed hand brace c) Real representation of the Arduino inside the case at the top of the 3D-printed hand brace.

2.3.3 Arduino Case and Inner Surface

For the incorporation of the sensors, wiring, and Arduino microcontroller, adjustments were made in the design of the 3D-printed hand brace. The Arduino microcontroller was enclosed with a two-part 3D-printed case manufactured with TPU 95A (white) in CURA. This protective case assured the microcontroller's safety and proper operation while being compatible with the hand brace's overall design and materials (**Figure 8** c).

Additionally, to increase functionality and maximize user comfort, a two-part 1mm-thick inner surface was 3D printed with TPU 95A (black) in CURA and incorporated into the design of the 3D-printed hand brace. The latter was inserted inside the brace to protect the skin from direct contact with the cables while it enabled the cleaning of the brace, which was crucial in instances of excessive perspiration. This inner surface served as a barrier, preventing skin irritation, and guaranteeing a comfortable wearing experience (**Figure 9**).

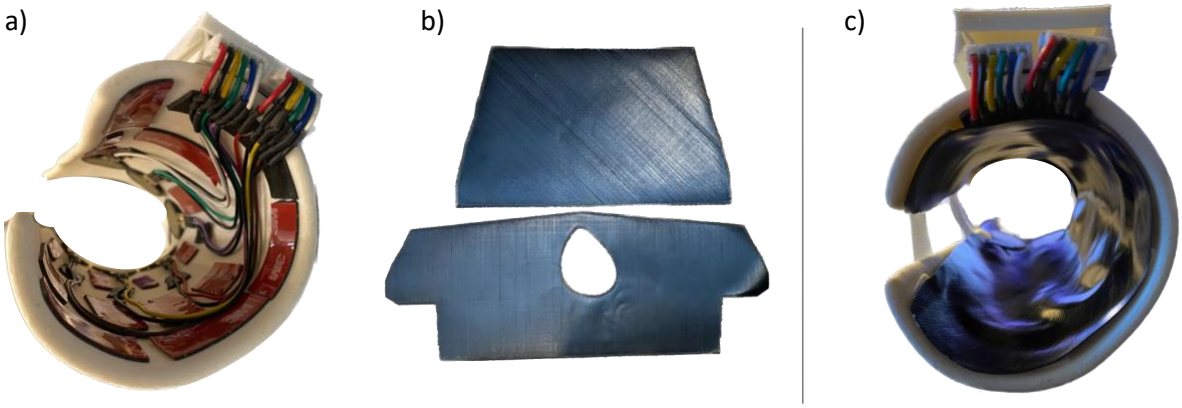

Figure 9. a) Placing wires and FSRs inside the 3D-printed hand brace, b) 3D-printed inner surface c) 3D-printed inner surface inside the 3D-printed hand brace to cover the cables.

2.4 Finite Element Analysis

Following up the design and manufacturing process of the 3D-printed hand brace, the fabrication and incorporation of electronics for the evaluation of brace, an FEA was conducted. Particularly, to investigate the contribution of the 3D-printed hand brace to the immobilization of the wrist joint under two loading scenarios, flexion, and extension, two finite element models were constructed: one with the 3D-printed hand brace and one without it.

2.4.1 Geometry Definition – Validation of the FEM

The initial step for the implementation of a detailed computational model required the geometries of the skeletal system, skin, and brace. The digital model of the hand brace was obtained as described in the previous section 2.2. Conversely, the 3D bone structures of the skeletal system, including the arm and hand, were designed in Blender. This approach was necessitated since the scanning process in this thesis, utilizing a smartphone, did not provide such geometries. These geometries had to be simplified to reduce the computational load, improve smoother design iterations, and ensure that the final brace model fitted exactly on the digital forearm model of section 2.2. Furthermore, the skin model was also designed in blender based on the digital forearm model from section 2.2. The validity of this simplification approach was confirmed through its application within a similar multi-step workflow involving an alternate brace, with a comprehensive discussion of this verification provided in the results section.

2.4.2 Design Procedure

Initially, the geometries of the skeletal system was obtained from an open CT database and then, processed by using image analysis software, Mimics. The design workflow of the arm model and the hand were completed in blender as follows:

- Design simple geometric shapes likes cylinders and planes and place them inside the existing geometries (**Figure 10** a, d)
- Edit vertices of each cylinder and align them with the geometry of each bone (**Figure 10** b, e)
- Use subdivision and Boolean modifiers to merge all the simplified shapes and create the simplified bones for ulna, radius, hand and fingers
- The final simplified models are detailed in the (**Figure 10** c, f)

In addition, the process to create the skin model was done in two stages. The first stage involved the merge of hand and arm in order to be used as an internal surface for the design of the skin (**Figure 10** g). Then, the second stage was to combine the outer skin from the section 2.2 with the internal surface to create the volume inside the skin (**Figure 10** h).

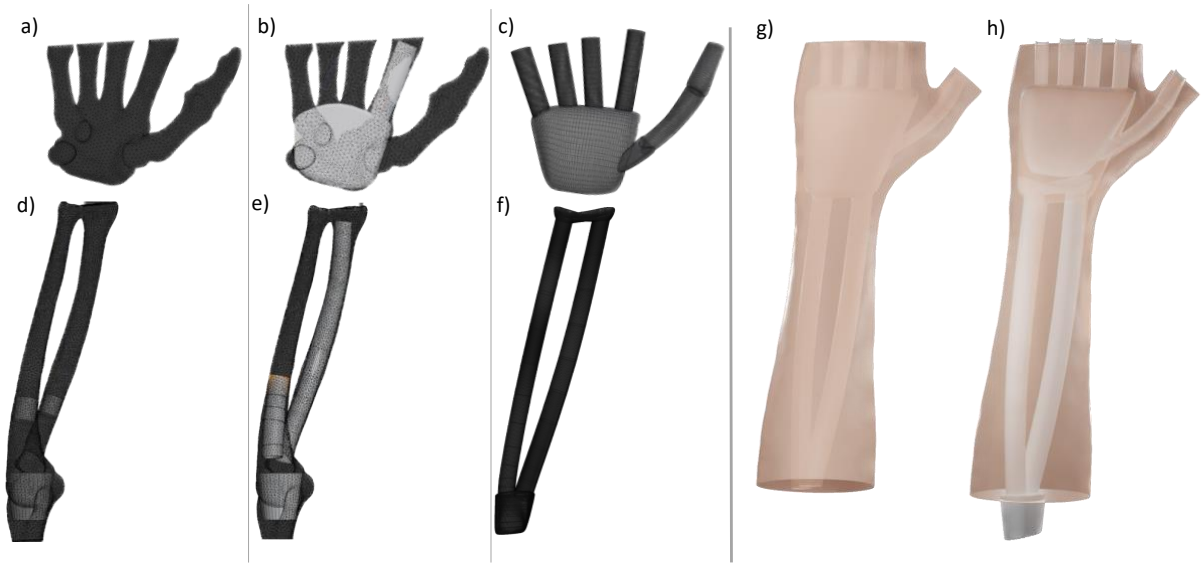

Figure 10. Render of the front view of the 3D bone structures in blender a) to f) simplified process of hand and arm, g) connected simplified arm and hand models to design the simplified skin and h) assembly of the arm, hand, and skin.

2.4.3 Material Assignment

In Abaqus, the material selection is one of the crucial steps and in this thesis, the mechanical properties of the bone structures, the hand and arm, were determined based on the median values found in literature [54]. Although the cancellous portion of the bone was not explicitly taken into consideration, the overall bone was allocated the properties of cortical bone with slightly reduced values to account for this assumption. The material properties of the skin were determined based on literature [55],[56],[57]. The TPU material properties such as Young's modulus and Poisson's ratio were also extracted from the literature [58]. **Table 2** provides a comprehensive listing of the material properties used in FEM.

Table 2. Mechanical properties of the parts considered in the FEA.

Parts	Young's modulus [MPa]	Poisson's ratio [-]
Bone	16000	0.3
Skin	0.3	0.45
Hand brace (TPU)	26	0.4

2.4.4 Mesh Generation

Regarding the mesh generation of the models of arm, hand, skin, and hand brace, it was conducted in GMSH, a free mesh generation software. Particularly, the first step involved employing the adaptive remesh option, whereby all parts underwent remeshing in accordance with the desired surface mesh seed size. Subsequently, volume meshes were added to all four parts of the FEM, and the mesh quality was evaluated to ensure the simulations were accurate.

2.4.5 Interactions

The next step of the FEM in Abaqus was to define the interactions between the four objects. More specifically, for the hand brace, a tie constraint was created between the outer skin surface (designated as the master surface) and the inner skin surface (designated as the slave surface). Tying bone and tissue is a common technique found in the literature [59]. For the interaction between the skin and the brace, a finite sliding surface-to-surface contact was defined. For the normal behavior, the 'hard contact' was used and for the tangential behavior, and the penalty method was selected with friction coefficient at 0.7. In the next step, a closing mechanism of the brace was added with the coupling of the two sides of the brace. For this purpose, a reference point was defined at the opening part of the brace at the wrist and at the end of the brace established for the straps. Then a chained wire, red line in **Figure 11** a, was defined between each two reference points to represent the connecting strap. A translational constraint named "link" was assigned to this wire. This link constraint keeps the distance between nodes constant and representation of a real tightened strap. In **Figure 11** a, the yellow circles are tie constraints, yellow squares are contact definition, and red dots indicate the modelled strapping [60],[61].

To simulate the rotation at the radiocarpal joint, the distal portion of the radius bone of the forearm and the first row of carpal bones in the lower hand are connected with a UJOINT connector that resembles the functionality of the wrist. Therefore, two reference points (RP), one close to the radius and the other one at the volumetric centre of the capitate bone on the hand were defined. Nodes at the distal portion of the radius were coupled to the closest RPs, and nodes of carpal bones are coupled to the other RP. A wire was defined connecting both reference points as the starting and end points (**Figure 11** b). Then a UJOINT connector, which is a kinematic constraint, was assigned to this wire. Afterward, the coordinate system of the connector was set and aligned with the rotation axis of the hand. One axis coincides with the created wire between the RPs of the hand and the arm. Since the UJOINT allows only rotations of UR1 (around the X-axis) and UR3 (around the Z-axis), the coordinate system was further defined such that the X axis was the axis for flexion and extension (**Figure 11** b). Also, the wrist is surrounded by ligaments that provide support and stability for the wrist and control the movement of the wrist. Rotational springs can be used to represent these ligaments and control the degree of freedom of the wrist. In this thesis, two rotational springs with stiffness of 10000 N/mm in direction X and Z were assigned to the wrist connector to constrain the range of motion at this joint.

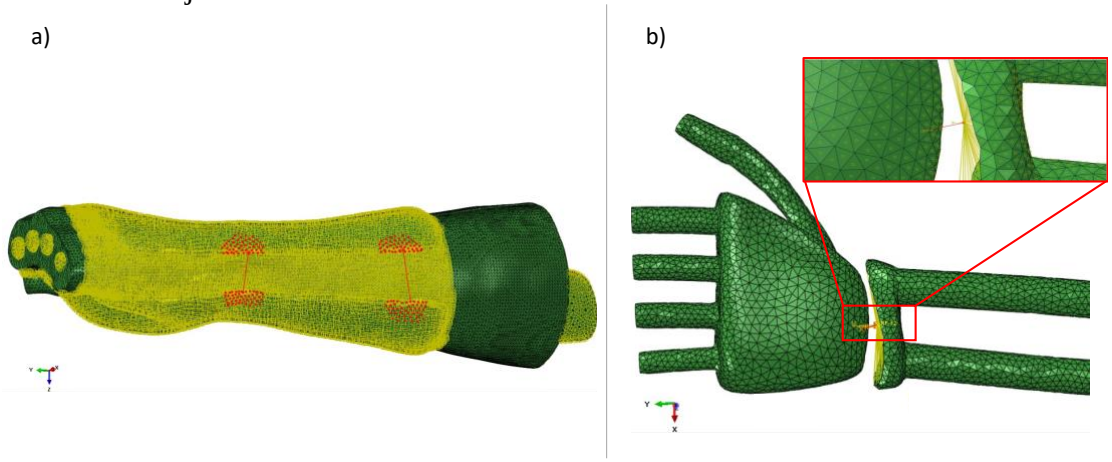

Figure 11. a) Defined interactions in the 3D-printed hand brace model, b) UJOINT connecting both bones, representing wrist movements via the hand reference points.

2.4.6 Boundary and Load Conditions

Regarding the boundary conditions of the FEM, constraints on the proximal end of the radius and ulna were imposed, as well as on the proximal end of the brace. The primary objective of a hand brace was to provide stabilization and restrict movement of the wrist joint, allowing patients to engage in their regular daily activities. In this study, an assessment of the brace's performance was conducted under two distinct load conditions: flexion, extension (**Figure 12**).

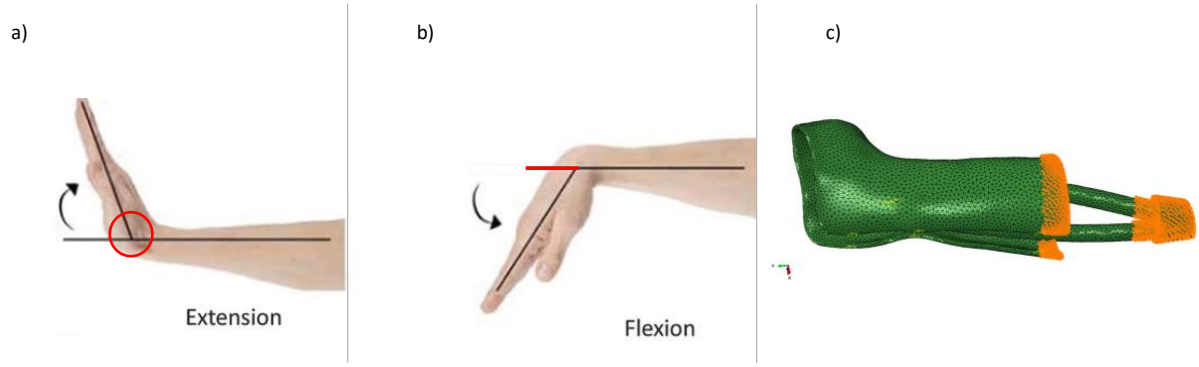

Figure 12. a and b) The movements of wrist: extension and flexion [62], c) Boundary conditions applied to the 3D-printed hand brace and the bone.

In the context of load conditions, a rotating motion was performed on the wrist joint using the specified hand reference points in the models (**Figure 12** a red circle) in the absence of the brace. Based on available empirical data, it has been shown that patients afflicted with arthritis have a reduced ability for rotational movement in comparison to those unaffected by the disease [57], [61], [63], [64].

Following this, the reaction moments was calculated by the equation:

$$M= F*X \quad (3)$$

where M represents the moment of wrist rotation, F indicates the weight, and X signifies the perpendicular distance between the line of action of the force and the reference point (**Figure 12** b red line), which has been measured to be 7 centimeters. The weight range included values ranging from 1 to 10kg, with the selection criteria being the force necessary for individuals to carry out their daily activities [65].

2.5 Experiment

An experiment was conducted to assess the functionality and efficacy of the 3D-printed hand brace. In parallel, an FEM was performed to replicate the distribution of contact pressure on the hand of a healthy adult participant to gain insight into the pressure distribution at the contact region under the 3D-printed hand. More specifically, an FEM was implemented using Abaqus, as outlined in Section 2.4 including the 3D-printed hand brace, arm, hand, skin and the sensors. The boundary and load conditions for the FEM were adjusted to replicate the experimental setup. The findings obtained from the experiment were compared with those obtained from computer simulations and then analyzed in the following sections.

Furthermore, numerous procedures were implemented to ensure the correspondence between the two models, FEM and the experimental setup. Initially, the distance denoted as X in the equation 3 was measured in order to accurately depict the interaction between the 3D-printed hand brace and the wrist in a more realistic way. In addition, in the FEM, the FSRs were defined as nodes based on the dimensions obtained from the physical FSRs. Following this, all the FSRs in Abaqus were positioned at the same locations as the FSRs inside the 3D-printed hand brace. Hence, the active region of the physical FSR and the red nodes (**Figure 13** a) in the computational model were identical (**Figure 13**).

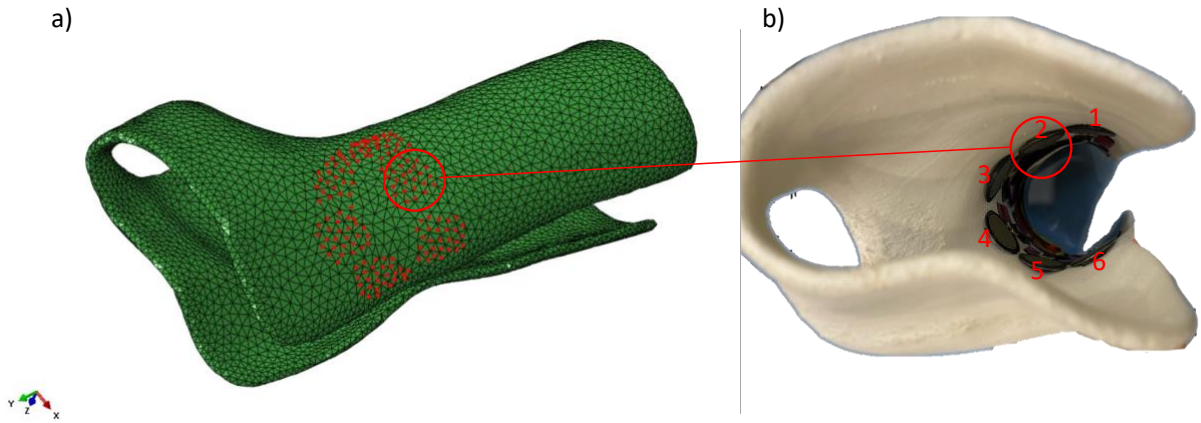

Figure 13. The positions of the six FSRs models inside a) the brace in Abaqus, b) inside the 3D-printed hand brace.

During the experiment, a healthy adult participant wore the 3D-printed hand brace with the integrated sensors. The experiment was to execute wrist flexion and extension movements under different loads while the elbow and the end of the 3D-printed hand brace were fixed to assure consistent conditions. The measurements derived from the six FSRs were recorded, yielding valuable information regarding the pressure distribution of the hand brace during movement.

To analyze the data in FEM, the average pressure was calculated by measuring all the pressure points at the active area of each sensor. Then, the output pressure of each FSR was converted to pressure (MPa) and recorded for the reasons of this analysis. **Figure 14** depicts an example of wrist flexion and also illustrates the process of collecting data from sensor 1 during experiment and the subsequent conversion of this value to MPa using equations (1) and (2) for further analysis.

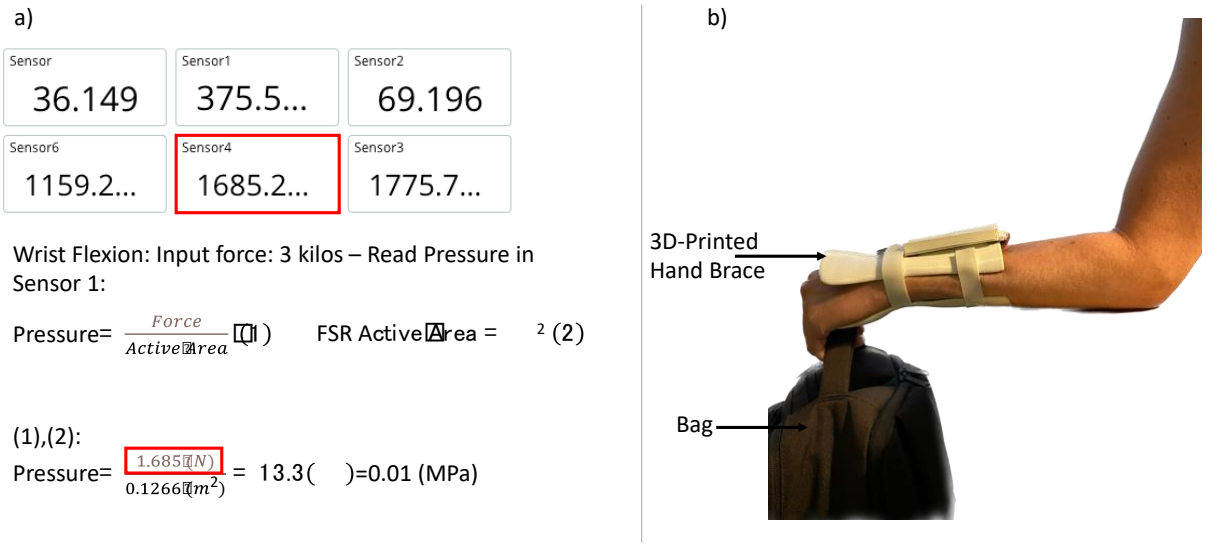

Figure 14. a) Pressure values from the six sensors as outlined in dashboard, as well as the equations of how to convert force to pressure, b) the 3D-printed hand brace that is worn by a participant and an object that was used to carry the weights for the experiment.

2.6 Post-Processing – Dashboard Design

In parallel with the experiments and FEM, a dashboard was developed inside the Arduino IoT Cloud. This dashboard made use of the connectivity features of the Arduino MKR 1010 microcontroller, enabling wireless Wi-Fi communication with the FSRs, and providing a user-friendly UI through a website and an application for smartphones for both patients and clinicians. The dashboard was designed to collect and display relevant data on the usage and the applied pressure of the 3D-printed hand brace on the wrist area. Two primary variables were incorporated into the dashboard: one to measure the time and the other to measure the pressure.

Six variables were used to detect and monitor the force exerted on each FSR. These variables recorded the force applied to each sensor for every second, providing a real-time indication of the 3D-printed hand brace's pressure distribution. By documenting and displaying these pressure values, patients could gain insight into the pressure levels and make any necessary adjustments to the straps, like tightening or loosening the strap based on the indications at the website or the app at their phones.

Moreover, four more variables were established in dashboard, each encompassing a range of values derived from the pressure data collected from the FSRs at one-second periods. The four variables were denoted as modes: "Relax," "Light," "Medium," and "Tight," each representing distinct levels of pressure by simulating the degree of tightness or looseness indicated by the straps. The thresholds of each mode determined during the experiment where the participant adjusted the straps to achieve varying comfort levels, enabling the calibration of pressure ranges for each of these modes. Consequently, the participant had the ability to promptly identify the operational mode of the hand brace and proceed to modify the straps by directly advising the phone application or the website.

One of the main challenges of this thesis was to create a system that informs the patient about the wearing time of the brace and encourage them to adhere at the prescribed treatment. For this reason, a real-time alert system was set inside the dashboard to notify the patient every time that they need to wear the brace for more time, or the applied pressure is insufficient or excessive based on the patient's comfort levels. The following sections provide a comprehensive explanation of the data related to the findings of this thesis.

3

Results

After iterating and prototyping multiple times, the final design of the 3D-printed hand brace was evaluated and fully manufactured. The outcomes of this process are reported in section 3.1. Subsequently, the design's performance is assessed through the FEA. In the last section, the experimental data are presented.

3.1 Assembly Overview

3.1.1 3D-Printed Hand Brace

The development of the 3D-printed hand brace necessitated a series of iterative and prototype-driven stages, ultimately resulting in the final version displayed in **Figure 15**. One notable characteristic of this design is the use of TPU exclusively for all components, including the main brace, straps, case, and interior surface, ranging in thickness from 1mm to 4mm. The choice of TPU as the primary material was crucial in ensuring that the brace conformed to the design criteria described in this thesis.

Table 3 summarizes the printing time and the material weight of all the fabricated parts. The weight of an orthotic device is a significant consideration due to the extended duration of patient usage. Currently, the 3D-printed hand brace has a total weight of 225g.

Table 3. Printing time [min] and material weight [g] for all parts

Parts	3d-printing time [min]	Material [g]
Hand brace	1920	90.2
Straps	82	3.2
Arduino case	302	12.9
Inner surface	134	7.9
Total (including electronics)	-	225

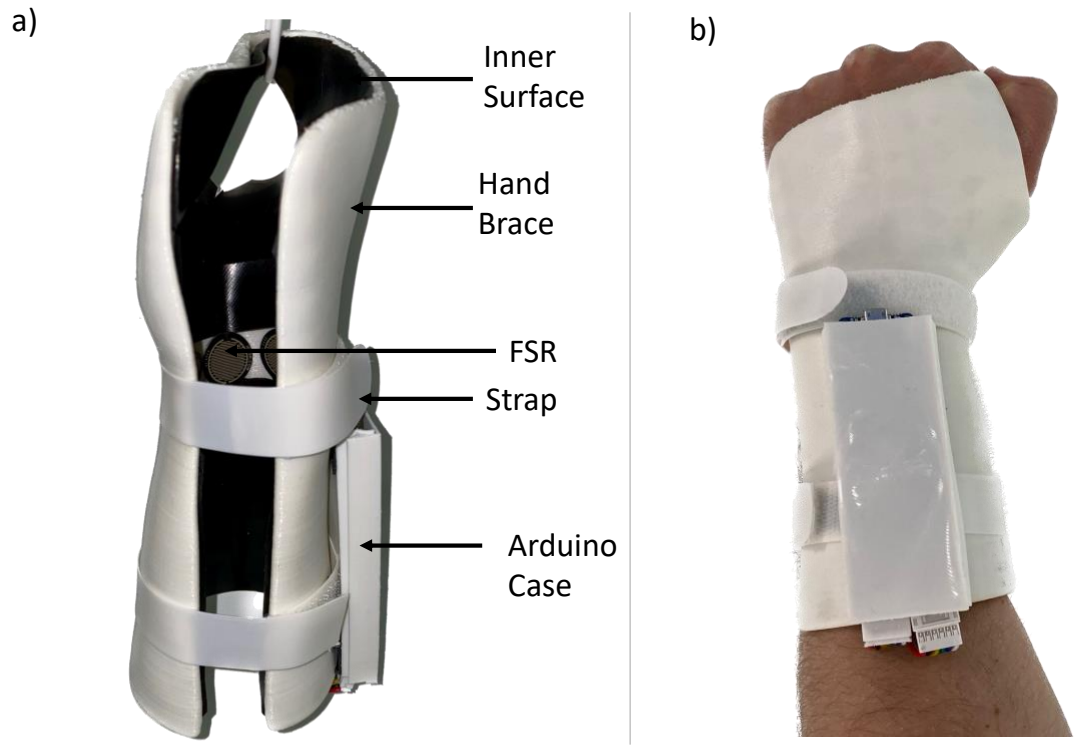

Figure 15. a) Overview of the 3D-printed hand brace b) Overview of the 3D-printed hand brace on the participant's hand.

3.1.2 Validation Procedure - 3D Bone Geometries

The results of the validation procedure for the simplification method applied to the 3D bone geometries indicate a difference percentage of 2.77%. This percentage was calculated based on the analysis of the maximum von Mises stresses recorded during wrist motion. Particularly, the complicated model exhibited maximum stress measurements ranging from 3.55MPa to 3.87 MPa, while the simplified model recorded stress values within the range of 3.45 MPa to 3.77 MPa (as illustrated in **Figure 16**).

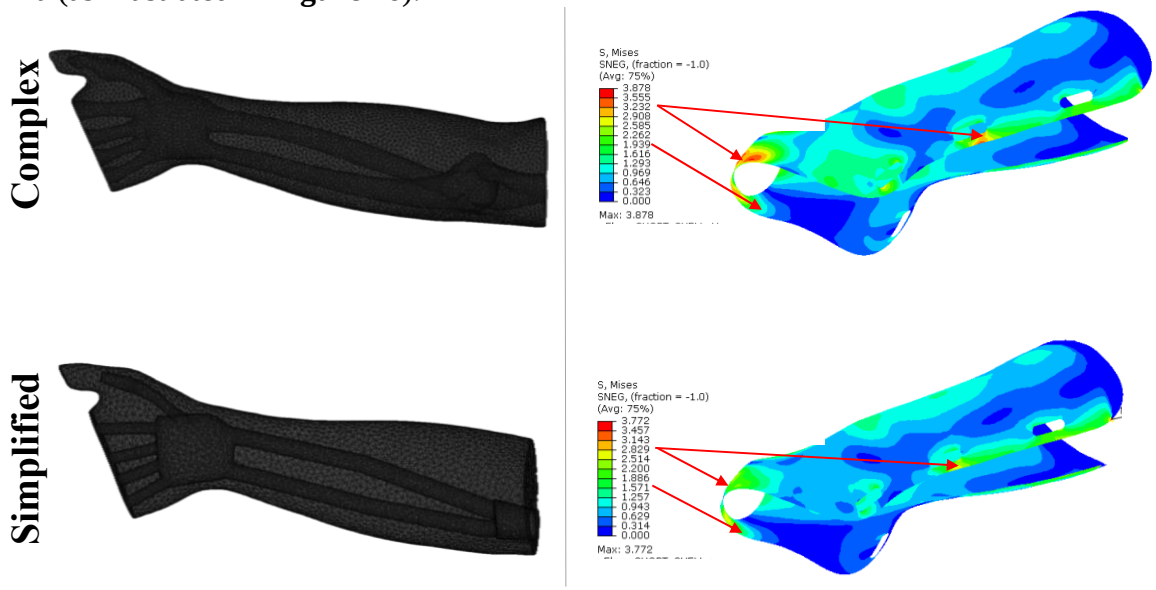

Figure 16. Render of the complex and simplified 3D bone geometries and the maximum Stress values in Abaqus during wrist movement (red arrows indicate the area of the maximum stress values).

3.2 Post-Processing

3.2.2 Finite Element Analysis

Once the design of the 3D-printed hand brace was finalized, the next step was to assess its performance through the data that was retrieved from the FEA. This FEA was served as a measurement tool of the hand rotation angles with and without the brace. These data allowed for a comprehensive analysis of the 3D-printed hand brace's effect on the wrist joint immobilization. The immobilization percentages were 84% with 6.8 degrees hand rotation and 85% with 5.7 degrees (**Figure 17**) for extension and flexion, respectively. In addition, the maximum von Mises stress on the brace was measured to be 1.6 MPa during extension, and 1.3 MPa during flexion (**Figure 17**), which were substantially less for both wrist movements than the yield stress of the TPU 95A (52.4MPa), ensuring safety during use.

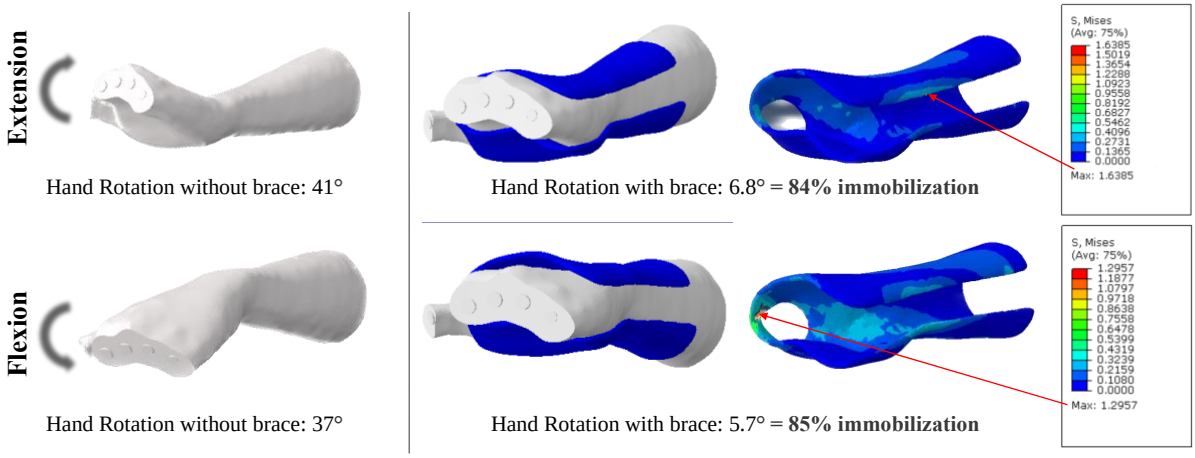

Figure 17. The percentage of immobilization under extension (top) and flexion (bottom) and the distribution of the von Mises stress (MPa) of the deformed 3D-printed hand brace for both wrist movements.

In parallel, this thesis focused to pressure distribution to assess the participant's comfort. Particularly, the primary factor influencing the level of comfort experienced when wearing a brace is the level of pressure applied to the forearm, which has a direct effect on the overall user satisfaction.

The results obtained from the FEA yielded valuable findings on regions exhibiting, pressure above 0.03 MPa, as seen in figure **Figure 18** (light green color) during both wrist movements, indicated low comfort levels.

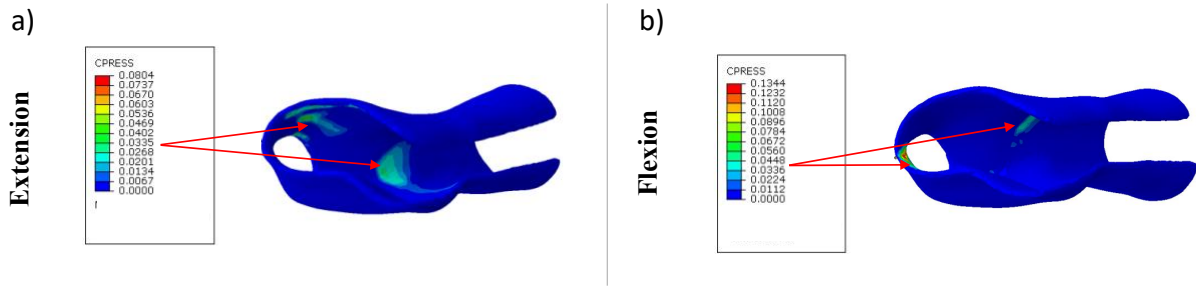

Figure 18. Pressure distribution (MPa) of the deformed 3D-printed hand brace for both wrist movements a) extension and b) flexion.

3.2.3 Comparison between FEM - Experiments

Once the data from the experiment and FEM were collected, an analysis was conducted to compare and examine them. During the experiment, it was noted that three FSRs were actually pressured based on their position inside the 3D-printed hand brace and so, the three sensors at top side of the brace were used for extension and other three for flexion. The comprehensive results, including relevant data on the minimum and maximum average pressure values observed are presented in both **Table 4** and **Table 5**.

Table 4. Pressure values from FRSs during extension wrist movement. EXP represents experiments.

Load [kg]	Sensor Number	Pressure [MPa]		Average Pressure [MPa]	
		FEM	**EXP**	**FEM**	**EXP**
1kg	1	0.19	0.05	**0.1**	**0.03**
	2	0.08	0.04		
	3	0.05	0.008		
2kg	1	0.2	0.17	0.11	0.12
	2	0.09	0.12		
	3	0.06	0.08		
3kg	1	0.24	0.16	0.14	0.15
	2	0.09	0.2		
	3	0.1	0.08		
4kg	1	0.25	0.17	0.15	0.15
	2	0.12	0.18		
	3	0.1	0.08		
5kg	1	0.27	0.21	0.16	0.14
	2	0.1	0.11		
	3	0.11	0.09		
6kg	1	0.31	0.20	0.19	0.20
	2	0.12	0.17		
	3	0.13	0.21		
7kg	1	0.34	0.23	**0.2**	**0.22**
	2	0.13	0.18		
	3	0.14	0.14		

Table 5. Pressure values from FRSs during flexion wrist movement. EXP represents experiments.

Load [kg]	Sensor Number	Pressure [MPa]		Average Pressure [MPa]	
		FEM	**EXP**	**FEM**	**EXP**
1kg	4	0.16	0.10		
	5	0.26	0.07	**0.22**	**0.07**
	6	0.23	0.05		
2kg	4	0.23	0.01		
	5	0.26	0.09	0.24	0.07
	6	0.24	0.12		
3kg	4	0.23	0.14		
	5	0.27	0.13	0.25	0.08
	6	0.26	0.09		
4kg	4	0.25	0.02		
	5	0.28	0.11	0.26	0.12
	6	0.26	0.12		
5kg	4	0.29	0.10		
	5	0.28	0.14	0.28	0.13
	6	0.26	0.15		
6kg	4	0.3	0.05		
	5	0.28	0.06	0.29	**0.15**
	6	0.27	0.33		
7kg	4	0.31	0.21		
	5	0.29	0.07	**0.3**	0.14
	6	0.29	0.12		

In **Table 4** and **Table 5**, the average pressure readings of sensors 1,2,3 as well as sensors 4,5,6 were collected and graphically represented in **Error! Reference source not found.**, which depicted the disparities between the two data sets of FEM and experiment. Specifically, the experiment recorded a maximum mean pressure value over 0.22 MPa, although in the FEM, it approached 0.3 MPa. During the experiment, the pressure values observed for extension ranged from 0.03 MPa to 0.22 MPa, whereas for flexion, the pressure values ranged from 0.07 MPa to 0.3 MPa. Additionally, it was observed that when the wrist motions reached a load of 8 kilos, the FSRs stopped working. Consequently, this threshold was established as the maximum applied force limit.

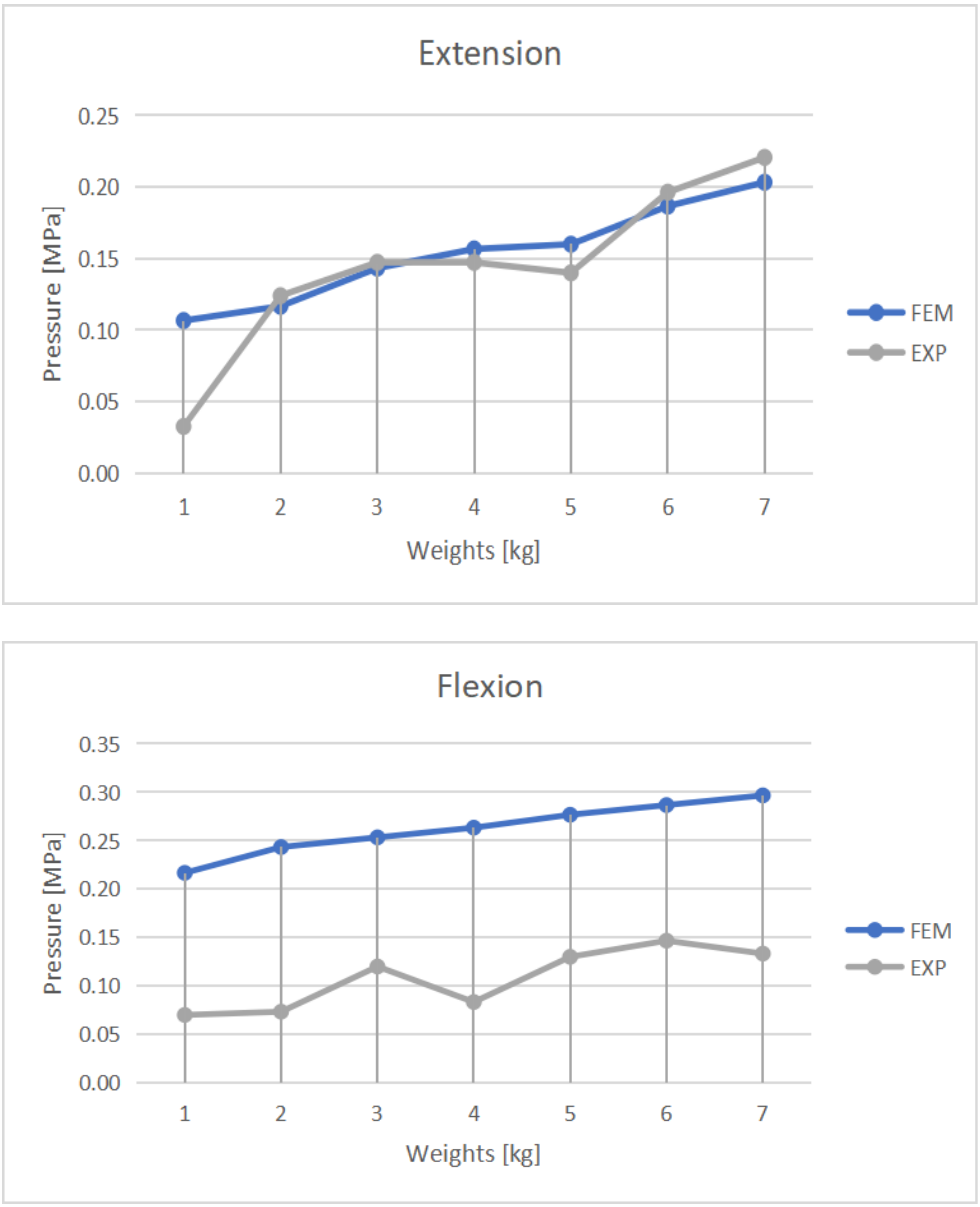

Figure 19. Comparison of the experiment and FEM, line plots of the wrist movements.

The correlation coefficients for extension and flexion wrist motions, which are 0.91 and 0.84 respectively, indicate a significant similarity in the patterns seen in **Error! Reference source not found.**. A comprehensive explanation of the two graphs can be found in the subsequent discussion section.

3.2.4 Dashboard

As it was already mentioned in methods, the dashboard was designed as an illustrative example, with customizable widgets, capable of serving as a reliable method for monitoring participants' adherence or nonadherence to wearing the orthosis as prescribed. In particular, the six FSRs inside the 3D-printed hand brace gathered pressure data, every time the hand brace was on the participant's hand. In this way, they could count both the wearing duration of the hand brace and remaining time based on the treatment plan as well as provided information about the applied pressure at the wrist.

Additionally, stickers were added to the dashboard to serve as reminders for each mode (**Figure 20** b, c), to deal with the aforementioned problems about the nonadherence to medical treatment programs, suggesting suitable activities for each level of tightness (e.g. each mode was recommended for a maximum of 4 to 6 hours per day). In addition to monitoring the brace's pressure, the interface also tracked the duration of usage in seconds, minutes and hours. The dashboard's code calculated and displayed the amount of time the patient wore the hand brace, as well as the remaining time in each mode (Relax, Light, Medium, and Tight). Taking into consideration that the six FSRs were placed in different positions around the wrist, and depending on the movement of the hand, each FSR unit was detecting different pressure values like "infinity" or "0.00053 N" (**Figure 20** f) when there is no pressure or almost no pressure on the sensor, respectively. Therefore, a variable was set to gain an insight about the pressure distribution and the average value of all the six FSRs were computed and imported into the code for categorization into one of the four different modes included in the dashboard.

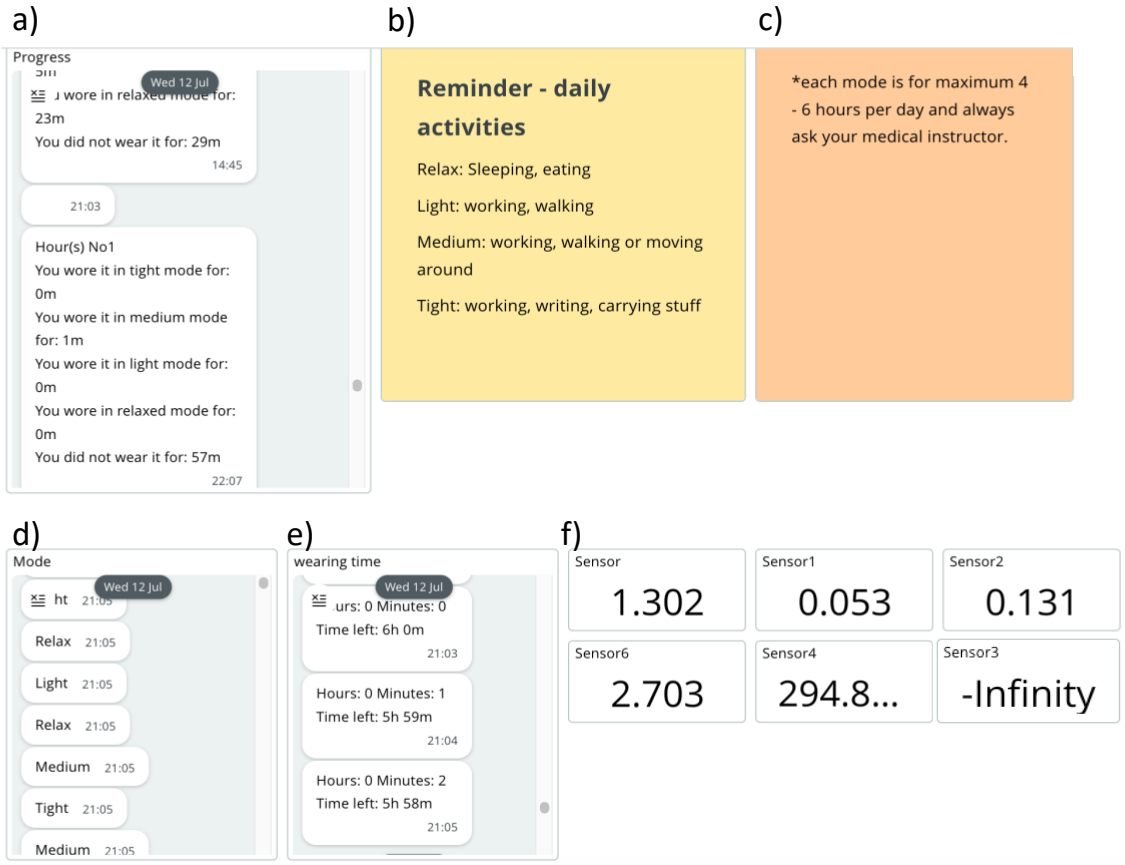

Figure 20. Overview of the Website UI in Arduino IOT cloud. a) Progress of wearing duration every 1 hour about the tightness of the 3D-printed hand brace. b – c) daily reminders of the treatment. d) Display the tightness of the brace on change. e) Monitor the time left. f) Display all the FSR pressure values on change.

4

Discussion

In this section, a comprehensive analysis of the findings and the limitations of this thesis were mentioned and recommendations for future research were provided highlighting the novel aspects of the hand brace design with integrated sensors.

Based on the literature, this is the first time that the design process of a 3D-printed hand brace with integrated FSRs for continuous monitoring of the brace's progress is reported. Consequently, it is challenging to make direct comparisons of the current workflow with the previous studies. In addition to the primary objective, which was to provide personalized feedback to patients and encourage them to adhere to the prescribed treatments, the design goals such as ensuring the hand brace's ergonomic compatibility with the participant's hand through the utilization of a flexible material and fostering a satisfactory level of comfort have been fulfilled based on the participant's feedback. An intriguing observation arises from the comparison of results between the experiments and FEA.

The FEA that was conducted to investigate the contact region inside the 3D-printed hand brace and evaluate its effectiveness in immobilizing the hand confirmed that the brace performed satisfactorily in providing support during motions of the wrist. Significantly, the brace exhibited an immobilization effectiveness surpassing 84% for wrist motions taking place at hand rotation angles of 6.8 degrees and 5.7 degrees. It is important to highlight that current clinical investigations often employ a criterion of 75% threshold in immobilization and hand rotation angles that are less than 10 degrees [38]. Additionally, the results obtained from the FEA provided useful information into identifiable areas in terms of pressure distribution and the stated comfort levels of the participant. According to the literature [49], any observations with pressure above 0.03 MPa, during both wrist movements indicate discomfort or potential areas of improvement. In the workflow of this thesis, adjustments in infill patterns during the 3D printing process were proposed to introduce flexibility and reduce the discomfort of the brace by modifying the infill density in these specific areas. The ultimate design of the 3D-printed hand brace was achieved, notably boosting the overall comfort experienced by the participant.

Moreover, discrepancies are particularly notable in the pressure values, with FEA indicating higher values. These findings warrant further examination, as discussed below. The analysis of the graph (**Error! Reference source not found.**) revealed an association between the wrist extension-flexion data obtained from the experiment and the FEA results. The data showed a good correlation between the experiment and FEA for various weights including 2,3,4,6 and 7 kg with small fluctuations for the 1kg and 5 kg and especially, for the experiment. The observed correlation may be due to several factors including simplifications and assumptions that made in the FEM. More specifically, the geometry of the hand and the arm were not obtained by

using one of the traditional scanning methods, like CT or MRI. Instead, both geometries were designed in Blender. The rationale for this approach was due to several reasons. Primarily, it aimed to minimize the participant's exposure to x-ray radiation, which was accomplished by utilizing smartphone-based methods. However, it's noteworthy that smartphones can capture only the external structure of the forearm and not the underlying skeletal bones. A simplification method was implemented to reduce the computational load and avoid segmentation process, while its verification was accomplished by comparing two FEMs, complex and simplified model. The resultant difference percentage was 2.77%, which is usually seen as a reliable indicator of good agreement in such analyses [66].

Furthermore, the discrepancy observed between the FEM and experimental results can be attributed, in part, to the structural differences between the CAD model of the brace and the actual 3D-printed hand brace used in the experiment. The CAD model had a uniform solid structure, whereas the 3D-printed brace was manufactured using various infill densities. Consequently, specific regions, notably at the palm, exhibited greater flexibility in the physical brace, leading to lose contact with the skin. Although, this increased flexibility allowed for greater hand movement freedom for the participant, compared to the controlled simulation in the FEM, it contributed to the observed fluctuations (**Table 4**, **Table 5**) as discussed below.

More specifically, these fluctuations occurred not only across different weights but also within the individual readings acquired from the FSRs. In the FEM, the individual FSRs average readings sometimes exhibited greater pressure values as the applied load increased. Conversely, in the experimental results, fluctuations in the sensor readings were particularly noticeable when evaluating weights of 4 kg and 5 kg during extension, as well as during the transition between 3 kg and 4 kg, and 6 kg and 7 kg during flexion. These fluctuations may be occurred due to two reasons. Firstly, the participant was responsible for securing the straps, and it became apparent that, with increasing weights, the fastening of the straps tended to become less secure. This resulted in a noticeable gap between the 3D-printed hand brace and the skin, subsequently leading to inadequate compression of FSRs. In addition, during a more detailed analysis of each FSR, it was noticed that the FSRs located near the open structure of the hand brace, namely FSRs 1 and 6 (**Figure 13**), showed higher pressure readings when the straps were tightened. This observation can be related to the continuous and direct contact between these FSRs and the skin.

Regarding the performance of the FSRs and the Arduino during the experiments, their reliability and consistency in terms of sensitivity and accuracy were proved. The sensors exhibited excellent performance during a continuous period of six months, reliably producing expected readings in accordance with their preset calibration. The development of the dashboard for reading FSRs and its features in relation to patient adherence is of great importance. This dashboard serves as a proof-of-concept, demonstrating its potential effectiveness. However, it is important to note that the values obtained from the sensors may differ across people. Nonetheless, the dashboard, along with its integrated features provides a foundation for future developments and allows patient-specific customization.

Having analyzed the findings and the disparities between experimental and simulated data, the focus now shifts towards the limits encountered during the development phases of the 3D-printed hand brace. Throughout the design process, multiple iterations were conducted to optimize the 3D-printed hand brace's functionality and several observations were noted that are worth mentioning. Firstly, the decision to use TPU 95A white filament for all parts, including the hand brace, straps, and case was driven by its aesthetically pleasing appearance. This

material effectively met the orthotic device's requirements for flexibility and immobilization. Notably, TPU allowed for high-quality 3D printing objects, and by altering the infill density, various levels of stiffness could be achieved. Additionally, the task of finely adjusting the printing settings to get the necessary outcomes might pose difficulties, particularly for clinicians. Secondly, the Arduino MKR 1010 was placed on top of the brace after considering and testing different positions, such as on the arm inside a separated case. The main concerns were the cable management and the replaceability of sensors. To address this, the case for Arduino was 3D-printed and combined with the pair of connectors for the sensors, allowing for optimal cable management and the ability to use the 3D-printed hand brace without the sensors.

Additionally, the use of adjustable 3D-printed straps facilitated patient-specific fitting. There are plenty options for closure mechanisms, and the selection of 3D-printed straps was done after testing various choices. Other options, like straps with embedded magnets or standard straps, were not suitable due to insufficient power for tightening or potential damage to the main brace caused by the applied force from standard straps. Hence, the optimal option was to manufacture the straps from the same material with brace. Finally, during the experiments, it was noted that the five FSRs stopped working and had to be replaced. The experiments were repeated with new FSRs, and the inner surface was 3D-printed and placed inside the brace. Two main factors contributed to this: the high load (over 8 kilos) and sweat inside the brace. All these iterations of the design ensured that the 3D-printed hand brace met the requirements for support, customization, and usability.

Despite the successful design of the 3D-printed hand brace, it is important to recognize its limitations including design and technical limitations, as well as providing several recommendations for future enhancements. Regarding the technical limitations of the design, the presence of electronic components such as the Arduino MKR 1010, the PCB, make the 3D-printed hand brace vulnerable to water and especially, to sweat. Therefore, patients should avoid wearing the brace in environments with high levels of moisture or when participating in water-based activities to prevent damaging the electronics. Another technical limitation of the design is battery life of the Arduino and the Wi-Fi communication. In particular, the integration of Wi-Fi communication for real-time data monitoring and cloud connectivity may pose challenges in terms of data security, energy consumption and the battery life which may vary based on usage frequency. Therefore, investigating alternative communication methods, such as Bluetooth communication, may offer the benefit of reduced energy consumption [67] while preserving the capacity for real-time data monitoring and communication. To achieve optimal performance, it is essential to strike a balance between power consumption and data transmission reliability.

As the first design of a 3D-printed hand brace with integrated sensors to be reported, further experimentation with the positioning and number of sensors can provide valuable insights about the pressure distribution and comfort levels of the orthosis. Understanding the distribution of pressure during various movements and activities will optimize the design of the brace for specific rehabilitation and treatment programs. The use of the existing FEA enables the potential advantages of contrasting a pressure map for the entire hand brace. Through the optimisation of sensors, clinicians may get a more thorough understanding of the impact of how the hand brace affects patient outcomes. Moreover, the 3D-printed hand brace may cause discomfort due to the accumulation of the perspiration between the brace and the skin. While the inner surface aids in providing a barrier, additional measures, such as topology optimization [68] to include ventilation in a later version may be required to overcome this

limitation. Although, topology optimization may add additional time to the current workflow as an extra step to the current workflow, it is a minor effect that can enhance the participant's overall experience in terms of comfort, ventilation, and fitness.

Lastly, the use of various TPU infill densities in the 3D-printed hand brace has shown promise. Nonetheless, experimentation with diverse infill patterns and materials may be required to provide a comparison between the current 3D-printed hand brace design with its future versions. Customizability and structural integrity of the hand brace can be improved by identifying the optimal combination that provides the greatest balance between support and mobility. This may encompass exploring alternative elastomers such as polyester or flexible resins, as well as employing diverse infill patterns like 3D cross that offer potential for a flexible model. Although the use of FSRs has demonstrated effectiveness in pressure measurement, their limitations in accuracy, +/- 2%, on complex geometries must be addressed. Notably, in this thesis, the integration of 3D-printed PLA plates facilitated precise sensor measurements. Despite the technical and design limitations, the 3D-printed hand brace with integrated sensors has presented a prospective pathway for further investigation and advancement.

5

Conclusion

In conclusion, this thesis has successfully demonstrated the design, development, and functional evaluation of a 3D-printed hand brace, offering potential applications in the possible treatment of forearm fractures. The present thesis has contributed to the field by comprehensively evaluating the brace's performance, particularly in terms of immobilization and wearer comfort, namely by using FEA in conjunction with experiments. The findings of this study contribute to comprehension of pressure distribution of the orthosis and the compliance monitoring, notably through wearable electronics. The interactive platform described in this thesis can easily be customized to each patient's need and can foster a collaborative approach to rehabilitation, where patients actively participate in their care, and clinicians have access to real time data for informed decision making.

References

[1]. BLAYA, F., PEDRO, P. S., SILVA, J. L., D'AMATO, R., HERAS, E. S. & JUANES, J. A. 2018. Design of an Orthopedic Product by Using Additive Manufacturing Technology: The Arm Splint. J Med Syst, 42, 54.

[2]. EL KHOURY, G., LIBOUTON, X., DE BOECK, F. & BARBIER, O. 2022. Use of a 3D-printed splint for the treatment of distal radius fractures: A randomized controlled trial. Orthopaedics & Traumatology-Surgery & Research, 108.

[3]. JANZING, H. M. J., BESSEMS, S. A. M., LIGTHART, M. A. P., VAN LIESHOUT, E. M. M., THEEUWES, H. P., BARTEN, D. G. & VERHOFSTAD, M. H. J. 2020. Treatment of dorsally dislocated distal radius fractures with individualized 3D printed bracing: an exploratory study. 3D Print Med, 6, 22.

[4]. KELLER, M., GUEBELI, A., THIERINGER, F. & HONIGMANN, P. 2021. Overview of In-Hospital 3D Printing and Practical Applications in Hand Surgery. Biomed Res Int, 2021, 4650245.

[5]. GORSKI, F., WICHNIAREK, R., KUCZKO, W., ZUKOWSKA, M., LULKIEWICZ, M. & ZAWADZKI, P. 2020. Experimental Studies on 3D Printing of Automatically Designed Customized Wrist-Hand Orthoses. Materials, 13.

[6]. HALE, L., LINLEY, E. & KALASKAR, D. M. 2020. A digital workflow for design and fabrication of bespoke orthoses using 3D scanning and 3D printing, a patient-based case study. Scientific Reports, 10.

[7]. KATT, B., IMBERGAMO, C., SEIGERMAN, D., RIVLIN, M. & BEREDJIKLIAN, P. K. 2021. The Use of 3D Printed Customized Casts in Children with Upper Extremity Fractures: A Report of Two Cases. Arch Bone Jt Surg, 9, 126-130.

[8]. HOWELL, D. M., BECHMANN, S. & UNDERWOOD, P. J. 2023. Wrist Splint. StatPearls. Treasure Island (FL).

[9]. GOLRIZ, B., AHMADI BANI, M., ARAZPOUR, M., BAHRAMIZADEH, M., CURRAN, S., MADANI, S. P. & HUTCHINS, S. W. 2016. Comparison of the efficacy of a neutral wrist splint and a wrist splint incorporating a lumbrical unit for the treatment of patients with carpal tunnel syndrome. Prosthet Orthot Int, 40, 617-23.

[10]. LIN, H., SHI, L. & WANG, D. 2015. A rapid and intelligent designing technique for patient-specific and 3D-printed orthopedic cast. 3D Print Med, 2, 4.

[11]. OUD, T. A. M., LAZZARI, E., GIJSBERS, H. J. H., GOBBO, M., NOLLET, F. & BREHM, M. A. 2021. Effectiveness of 3D-printed orthoses for traumatic and chronic hand conditions: A scoping review. PLoS One, 16, e0260271.

[12]. BEEKER, R. W. & REHMAN, U. H. 2023. Carpal Ligament Instability. StatPearls. Treasure Island (FL).

[13]. PALOUSEK, D., ROSICKY, J., KOUTNY, D., STOKLASEK, P. & NAVRAT, T. 2014. Pilot study of the wrist orthosis design process. Rapid Prototyping Journal, 20, 27-32.

[14]. PATERSON, A. M., BIBB, R., CAMPBELL, R. I. & BINGHAM, G. 2015. Comparing additive manufacturing technologies for customised wrist splints. Rapid Prototyping Journal, 21, 230-243.

[15]. PLINT, A., CLIFFORD, T., PERRY, J., BULLOCH, B., PUSIC, M., LALANI, A., ALI, S., NGUYEN, B. H., JOUBERT, G. & MILLAR, K. 2003. Wrist buckle fractures: a survey of current practice patterns and attitudes toward immobilization. CJEM, 5, 95-100.

[16]. POPESCU, D., ZAPCIU, A., TARBA, C. & LAPTOIU, D. 2020. Fast production of customized three-dimensional-printed hand splints. Rapid Prototyping Journal, 26, 134-144.
[17]. SCHWARTZ, D. A. & SCHOFIELD, K. A. 2021. Utilization of 3D printed orthoses for musculoskeletal conditions of the upper extremity: A systematic review. J Hand Ther.
[18]. VEEHOF, M. M., TAAL, E., WILLEMS, M. J. & VAN DE LAAR, M. A. F. J. 2008. Determinants of the use of wrist working splints in rheumatoid arthritis. Arthritis & Rheumatism-Arthritis Care & Research, 59, 531-536.
[19]. BARRIOS-MURIEL, J., ROMERO-SANCHEZ, F., ALONSO-SANCHEZ, F. J. & RODRIGUEZ SALGADO, D. 2020. Advances in Orthotic and Prosthetic Manufacturing: A Technology Review. Materials (Basel), 13.
[20]. REIS, P., VOLPINI, M., MAIA, J. P., GUIMARAES, I. B., EVELISE, C., MONTEIRO, M. & RUBIO, J. C. C. 2022. Resting hand splint model from topology optimization to be produced by additive manufacturing. Rapid Prototyping Journal, 28, 216-225.
[21]. LAZZERI, S., TALANTI, E., BASCIANO, S., BARBATO, R., FONTANELLI, F., UCCHEDDU, F., SERVI, M., VOLPE, Y., VAGNOLI, L., AMORE, E., MARZOLA, A., MCGREEVY, K. S. & CARFAGNI, M. 2022. 3D-Printed Patient-Specific Casts for the Distal Radius in Children: Outcome and Pre-Market Survey. Materials, 15.
[22]. FANG, J. J., LIN, C. L., TSAI, J. Y. & LIN, R. M. 2022. Clinical Assessment of Customized 3D-Printed Wrist Orthoses. Applied Sciences-Basel, 12.
[23]. SKIBICKI, H. E., KATT, B. M., LUTSKY, K., WANG, M. L., MCENTEE, R., VACCARO, A. R., BEREDJIKLIAN, P. & RIVLIN, M. 2021. Three Dimensionally Printed Versus Conventional Casts in Pediatric Wrist Fractures. Cureus, 13, e19090.
[24]. OUD, T., KERKUM, Y., DE GROOT, P., GIJSBERS, H., NOLLET, F. & BREHM, M. A. 2021. Production Time and User Satisfaction of 3-Dimensional Printed Orthoses For Chronic Hand Conditions Compared With Conventional Orthoses: A Prospective Case Series. J Rehabil Med Clin Commun, 4, 1000048.
[25]. HOOGERVORST, P., KNOX, R., TANAKA, K., WORKING, Z. M., EL NAGA, A. N., HERFAT, S. & LEE, N. 2020. A Biomechanical Comparison of Fiberglass Casts and 3-Dimensional-Printed, Open-Latticed, Ventilated Casts. Hand (N Y), 15, 842-849.
[26]. GRAHAM, J., WANG, M., FRIZZELL, K., WATKINS, C., BEREDJIKLIAN, P. & RIVLIN, M. 2020. Conventional vs 3-Dimensional Printed Cast Wear Comfort. Hand (N Y), 15, 388-392.
[27]. CHEN, Y., LIN, H., YU, Q., ZHANG, X., WANG, D., SHI, L., HUANG, W. & ZHONG, S. 2020. Application of 3D-Printed Orthopedic Cast for the Treatment of Forearm Fractures: Finite Element Analysis and Comparative Clinical Assessment. Biomed Res Int, 2020, 9569530.
[28]. CHEN, Y. J., LIN, H., ZHANG, X., HUANG, W., SHI, L. & WANG, D. 2017. Application of 3D-printed and patient-specific cast for the treatment of distal radius fractures: initial experience. 3D Print Med, 3, 11.
[29]. YAN, W., DING, M., KONG, B., XI, X. & ZHOU, M. 2019. Lightweight Splint Design for Individualized Treatment of Distal Radius Fracture. J Med Syst, 43, 284.
[30]. GUIDA, P., CASABURI, A., BUSIELLO, T., LAMBERTI, D., SORRENTINO, A., IUPPARIELLO, L., D'ALBORE, M., COLELLA, F. & CLEMENTE, F. 2019. An alternative to plaster cast treatment in a pediatric trauma center using the CAD/CAM technology to manufacture customized three-dimensional-printed orthoses in a totally hospital context: a feasibility study. J Pediatr Orthop B, 28, 248-255.

[31]. LI, J. & TANAKA, H. 2018. Rapid customization system for 3D-printed splint using programmable modeling technique - a practical approach. 3D Print Med, 4, 5.
[32]. KIM, S. J., KIM, S. J., CHA, Y. H., LEE, K. H. & KWON, J. Y. 2018. Effect of personalized wrist orthosis for wrist pain with three-dimensional scanning and printing technique: A preliminary, randomized, controlled, open-label study. Prosthetics and Orthotics International, 42, 636-643.
[33]. DEVANAND, D. B. & KEDGLEY, A. E. 2023. Objective Methods of Monitoring Usage of Orthotic Devices for the Extremities: A Systematic Review. Sensors (Basel), 23.
[34]. COLE, T., ROBINSON, L., ROMERO, L. & O'BRIEN, L. 2019. Effectiveness of interventions to improve therapy adherence in people with upper limb conditions: A systematic review. J Hand Ther, 32**,** 175-183 e2.
[35]. DAVIES, G., YEOMANS, D., TOLKIEN, Z., KREIS, I. A., POTTER, S., GARDINER, M. D., JAIN, A., HENDERSON, J. & BLAZEBY, J. M. 2020. Methods for assessment of patient adherence to removable orthoses used after surgery or trauma to the appendicular skeleton: a systematic review. Trials, 21**,** 507.
[36]. JACK, K., MCLEAN, S. M., MOFFETT, J. K. & GARDINER, E. 2010. Barriers to treatment adherence in physiotherapy outpatient clinics: a systematic review. Man Ther, 15**,** 220-8.
[37]. PICHA, K. J. & HOWELL, D. M. 2018. A model to increase rehabilitation adherence to home exercise programmes in patients with varying levels of self-efficacy. Musculoskeletal Care, 16**,** 233-237.
[38]. SAVAS, S. & AYDOGAN, C. 2022. Factors affecting orthosis adherence after acute traumatic hand tendon repairs: A prospective cohort study. J Hand Ther, 35**,** 32-40.
[39]. RIVETT, L., ROTHBERG, A., STEWART, A. & BERKOWITZ, R. 2009. The relationship between quality of life and compliance to a brace protocol in adolescents with idiopathic scoliosis: a comparative study. BMC Musculoskelet Disord, 10**,** 5.
[40]. BENISH, B. M., SMITH, K. J. & SCHWARTZ, M. H. 2012. Validation of a miniature thermochron for monitoring thoracolumbosacral orthosis wear time. Spine (Phila Pa 1976), 37**,** 309-15.
[41]. HUNTER, L. N., SISON-WILLIAMSON, M., MENDOZA, M. M., MCDONALD, C. M., MOLITOR, F., MULCAHEY, M. J., BETZ, R. R., VOGEL, L. C. & BAGLEY, A. 2008. The validity of compliance monitors to assess wearing time of thoracic-lumbar-sacral orthoses in children with spinal cord injury. Spine (Phila Pa 1976), 33**,** 1554-61.
[42]. TAKEMITSU, M., BOWEN, J. R., RAHMAN, T., GLUTTING, J. J. & SCOTT, C. B. 2004. Compliance monitoring of brace treatment for patients with idiopathic scoliosis. Spine (Phila Pa 1976), 29**,** 2070-4; discussion 2074.
[43]. AKIYAMA, Y., OKAMOTO, S., YAMADA, Y. & ISHIGURO, K. 2016. Measurement of Contact Behavior Including Slippage of Cuff When Using Wearable Physical Assistant Robot. IEEE Trans Neural Syst Rehabil Eng, 24**,** 784-93.
[44]. DZEDZICKIS, A., SUTINYS, E., BUCINSKAS, V., SAMUKAITE-BUBNIENE, U., JAKSTYS, B., RAMANAVICIUS, A. & MORKVENAITE-VILKONCIENE, I. 2020. Polyethylene-Carbon Composite (Velostat((R))) Based Tactile Sensor. Polymers (Basel), 12.
[45]. MACINNES, P., LEWIS, T. L., GRIFFIN, C., MARTINUZZI, M., SHEPHERD, K. L. & KOKKINAKIS, M. 2022. Surgical management of pes planus in children with cerebral palsy: A systematic review. J Child Orthop, 16**,** 333-346.
[46]. CHA, Y. J. 2018. Changes in the pressure distribution by wrist angle and hand position in a wrist splint. Hand Surg Rehabil, 37**,** 38-42.

[47]. BINELLI, M. R., VAN DOMMELEN, R., NAGEL, Y., KIM, J., HAQUE, R. I., COULTER, F. B., SIQUEIRA, G., STUDART, A. R. & BRIAND, D. 2023. Digital manufacturing of personalised footwear with embedded sensors. Sci Rep, 13**,** 1962.
[48]. CHALMERS, E., LOU, E., HILL, D., ZHAO, V. H. & WONG, M. S. 2012. Development of a pressure control system for brace treatment of scoliosis. IEEE Trans Neural Syst Rehabil Eng, 20**,** 557-63.
[49]. TAN, X., AHMED-KRISTENSEN, S., CAO, J., ZHU, Q., CHEN, W. & NANAYAKKARA, T. 2021. A Soft Pressure Sensor Skin to Predict Contact Pressure Limit Under Hand Orthosis. IEEE Trans Neural Syst Rehabil Eng, 29**,** 536-545.
[50]. TAN, X., AHMED-KRISTENSEN, S., CAO, J., ZHU, Q., CHEN, W. & NANAYAKKARA, T. 2021. A Soft Pressure Sensor Skin for Hand and Wrist Orthoses. IEEE Trans Neural Syst Rehabil Eng, 29**,** 536-545.
[51]. Interlink Electronics. FSR 400 Series Data Sheet. https://cdn2.hubspot.net/hubfs/3899023/Interlinkelectronics%20November2017/Docs/Datasheet_FSR.pdf.
[52]. Force Sensitive Resistors (FSRs) with Arduino: https://makersportal.com/blog/2020/5/24/force-sensitive-resistors-fsrs-arduino.
[53]. LUKASZEWSKI, K., WICHNIAREK, R. & GORSKI, F. 2020. Determination of the Elasticity Modulus of Additively Manufactured Wrist Hand Orthoses. Materials (Basel), 13.
[54]. CAGLE, J. C., REINHALL, P. G., ALLYN, K. J., MCLEAN, J., HINRICHS, P., HAFNER, B. J. & SANDERS, J. E. 2018. A finite element model to assess transtibial prosthetic sockets with elastomeric liners. Med Biol Eng Comput, 56**,** 1227-1240.
[55]. GUILLAUME BOISOT, C. FOND, GILLES HOCHSTETTER, LUCIEN LAIARINANDRASANA. 2008. Failure of polyamide 11 using a damage finite elements model. ECF 17, Brno, Czech Republic.
[56]. XU, Y. X. & JUANG, J. Y. 2021. Measurement of Nonlinear Poisson's Ratio of Thermoplastic Polyurethanes under Cyclic Softening Using 2D Digital Image Correlation. Polymers (Basel), 13.
[57]. CAZON, A., KELLY, S., PATERSON, A. M., BIBB, R. J. & CAMPBELL, R. I. 2017. Analysis and comparison of wrist splint designs using the finite element method: Multi-material three-dimensional printing compared to typical existing practice with thermoplastics. Proc Inst Mech Eng H, 231, 881-897.
[58]. TPU 95A FOR S SERIES. https://ultimaker.com/materials/s-series-tpu-95a/
[59]. HUA, Z., WANG, J. W., LU, Z. F., MA, J. W. & YIN, H. 2018. The biomechanical analysis of three-dimensional distal radius fracture model with different fixed splints. Technol Health Care, 26**,** 329-341.
[60]. RAINBOW, M. J., WOLFF, A. L., CRISCO, J. J. & WOLFE, S. W. 2016. Functional kinematics of the wrist. J Hand Surg Eur Vol, 41**,** 7-21.
[61]. RUBY, L. K., COONEY, W. P., 3RD, AN, K. N., LINSCHEID, R. L. & CHAO, E. Y. 1988. Relative motion of selected carpal bones: a kinematic analysis of the normal wrist. J Hand Surg Am, 13**,** 1-10.
[62]. PILLEMER, R. & SPRINGERLINK 2022. Handbook of Upper Extremity Examination : A Practical Guide, Cham, Springer International Publishing : Imprint: Springer.
[63]. AMIS, A. A., HUGHES, S., MILLER, J. H., WRIGHT, V. & DOWSON, D. 1979. Elbow joint forces in patients with rheumatoid arthritis. Rheumatol Rehabil, 18**,** 230-4.
[64]. VEEGER, H. E., MEERSHOEK, L. S., VAN DER WOUDE, L. H. & LANGENHOFF, J. M. 1998. Wrist motion in handrim wheelchair propulsion. J Rehabil Res Dev, 35**,** 305-13.

[65]. PAGNOTTA, A., KORNER-BITENSKY, N., MAZER, B., BARON, M. & WOOD-DAUPHINEE, S. 2005. Static wrist splint use in the performance of daily activities by individuals with rheumatoid arthritis. J Rheumatol, 32**,** 2136-43.
[66]. VICKERS, AJ. 2001. The use of percentage change from baseline as an outcome in a controlled trial is statistically inefficient: a simulation study. BMC Med Res Methodol, 1:6.
[67]. OLEH HORYACHYY. 2017. Comparison of Wireless Communication Technologies used in a Smart Home: Analysis of wireless sensors node based on Arduino in home automation scenario. Master Thesis, Faculty of Computing, Blekinge Institute of Technology.
[68]. YUNBO, Z., TSZ-HO., K. 2019. Customization and topology optimization of compression casts/braces on two-manifold surfaces. Computer-Aided Design, 111, 113-122.

Appendix A

Arduino Code

The following variables are automatically generated and updated when changes are made to the Thing:

```
  String mode;
  String progress;
  String wearing_time;
  float fsrForce;
  float fsrForce1;
  float fsrForce2;
  float fsrForce3;
  float fsrForce4;
  float fsrForce6;


#include "thingProperties.h"

int fsrPin = 0;     // the FSR and 4.7kohm pulldown are connected to a0
int fsrReading;     // the analog reading from the FSR resistor divider
int fsrVoltage;     // the analog reading converted to voltage
unsigned long fsrResistance;  // The voltage converted to resistance, can be very big so make "long"
unsigned long fsrConductance;
//float fsrForce;       // Finally, the resistance converted to force

int fsrPin1 = 1;
int fsrReading1;
int fsrVoltage1;
unsigned long fsrResistance1;
unsigned long fsrConductance1;
//float fsrForce1;

int fsrPin2 = 2;
int fsrReading2;
int fsrVoltage2;
unsigned long fsrResistance2;
unsigned long fsrConductance2;
//float fsrForce2;

int fsrPin3 = 3;
int fsrReading3;
int fsrVoltage3;
unsigned long fsrResistance3;
unsigned long fsrConductance3;
```

```
//float fsrForce3;

int fsrPin4 = 4;
int fsrReading4;
int fsrVoltage4;
unsigned long fsrResistance4;
unsigned long fsrConductance4;
//float fsrForce4;

int fsrPin6 = 6;
int fsrReading6;
int fsrVoltage6;
unsigned long fsrResistance6;
unsigned long fsrConductance6;
//float fsrForce6;

float a1 = 26974849;
float a2 = -1.2968;

int mode1 = 5;
int mode2 = 100;
int mode3 = 170;
int mode4 = 300;

int hours = 0;
int minutes = 0;
int count = 0;
int median_force = 0;
int median_fsr_reading = 0;

int target = 360;
int total_minutes_left = 0;
int minutes_left = 0;
int hours_left = 0;

int reporting_count = 1;
int mode4_count = 0;
int mode3_count = 0;
int mode2_count = 0;
int mode1_count = 0;
int not_wearing_count = 0;
int hours_count = 0;

#include <WiFiNINA.h>

char ssid[] = "";      // your network SSID (name)
char pass[] = "";    // your network password
int status = WL_IDLE_STATUS;

void setup() {
```

```
  // Initialize serial and wait for port to open:
  Serial.begin(9600);
  // This delay gives the chance to wait for a Serial Monitor without blocking if none is found
  delay(1500);

 //attempt to connect to WiFi network
  while (status != WL_CONNECTED) {
    Serial.print("Attempting to connect to SSID: ");
    Serial.println(ssid);
    status = WiFi.begin(ssid, pass);
    delay(5000);
  }

  // print WiFi status
  Serial.println("Connected to wifi");
  printWiFiStatus();
  // Defined in thingProperties.h
  initProperties();

  // Connect to Arduino IoT Cloud
  ArduinoCloud.begin(ArduinoIoTPreferredConnection);


  setDebugMessageLevel(2);
  ArduinoCloud.printDebugInfo();
}

void loop() {
  ArduinoCloud.update();
  // Your code here
  fsrReading = analogRead(fsrPin);

  fsrReading1 = analogRead(fsrPin1);

  fsrReading2 = analogRead(fsrPin2);

  fsrReading3 = analogRead(fsrPin3);

  fsrReading4 = analogRead(fsrPin4);

  fsrReading6 = analogRead(fsrPin6);


 fsrVoltage = map(fsrReading, 0, 1023, 0, 3300);
 fsrResistance = ((3300 - fsrVoltage) * 4700) / fsrVoltage; // fsrVoltage is in millivolts so 5V
= 5000mV
 fsrForce = a1 * pow(fsrResistance, a2);

 fsrVoltage1 = map(fsrReading1, 0, 1023, 0, 3300);
 fsrResistance1 = ((3300 - fsrVoltage1) * 4700) / fsrVoltage1;
```

```
 fsrForce1 = a1 * pow(fsrResistance1, a2);

 fsrVoltage2 = map(fsrReading2, 0, 1023, 0, 3300);
 fsrResistance2 = ((3300 - fsrVoltage2) * 4700) / fsrVoltage2;
 fsrForce2 = a1 * pow(fsrResistance2, a2);

 fsrVoltage3 = map(fsrReading3, 0, 1023, 0, 3300);
 fsrResistance3 = ((3300 - fsrVoltage3) * 4700) / fsrVoltage3;
 fsrForce3 = a1 * pow(fsrResistance3, a2);

 fsrVoltage4 = map(fsrReading4, 0, 1023, 0, 3300);
 fsrResistance4 = ((3300 - fsrVoltage4) * 4700) / fsrVoltage4;
 fsrForce4 = a1 * pow(fsrResistance4, a2);

 fsrVoltage6 = map(fsrReading6, 0, 1023, 0, 3300);
 fsrResistance6 = ((3300 - fsrVoltage6) * 4700) / fsrVoltage6;
 fsrForce6 = a1 * pow(fsrResistance6, a2);

 mean_fsr_reading = (fsrReading + fsrReading1 + fsrReading2 + fsrReading3 + fsrReading4
+ fsrReading6) / 6;
 mean_force = (fsrForce + fsrForce1 + fsrForce2 + fsrForce3 + fsrForce4 + fsrForce6) / 6;

 if(mean_fsr_reading >= mode4) {
   mode = "Tight";
   mode4_count++;
 }
else if(mean_fsr_reading >= mode3) {
   mode = "Medium";
   mode3_count++;
 }
else if(mean_fsr_reading >= mode2) {
   mode = "Light";
   mode2_count++;
 }
 else if(mean_fsr_reading >= mode1) {
   mode = "Relax";
   mode1_count++;
 }
 else {
   mode = "Not wearing";
   not_wearing_count++;
 }

 if (mode != "Not wearing") {
  count = count + 1;
  hours = count / 3600;
  minutes = (count % 3600) / 60;
 }

 total_minutes_left = target - ((hours * 60) + minutes);
```

```
 hours_left = total_minutes_left / 60;
 minutes_left = total_minutes_left % 60;
 wearing_time = String("Hours: ") + hours + " Minutes: " + minutes + "\n" + "Time left: " +
hours_left + "h " + minutes_left + "m";

 reporting_count++;
 if(reporting_count == 3600) {
   hours_count++;
   mode4_count = mode4_count / 60;
   mode3_count = mode3_count / 60;
   mode2_count = mode2_count / 60;
   mode1_count = mode1_count / 60;
   not_wearing_count = not_wearing_count / 60;
  progress = String("Hour(s) No") + hours_count + "\n"+ "You wore it in tight mode for: " +
mode4_count + "m\n"+ "You wore it in medium mode for: "+ mode3_count + "m\n"+ "You
wore it in light mode for: "+ mode2_count + "m\n" + "You wore in relaxed mode for: " +
mode1_count + "m\n"+ "You did not wear it for: " + not_wearing_count + "m";
   reporting_count = 1;
   mode4_count = 0;
   mode3_count = 0;
   mode2_count = 0;
   mode1_count = 0;
   not_wearing_count = 0;
  }

  delay(1000);

}

void printWiFiStatus() {
  // print the SSID of the network you're attached to
  Serial.print("SSID: ");
  Serial.println(WiFi.SSID());

  // print your board's IP address
  IPAddress ip = WiFi.localIP();
  Serial.print("IP Address: ");
  Serial.println(ip);

  // print the received signal strength
  long rssi = WiFi.RSSI();
  Serial.print("signal strength (RSSI):");
  Serial.print(rssi);
  Serial.println(" dBm");
}
```

Appendix B

Assembly

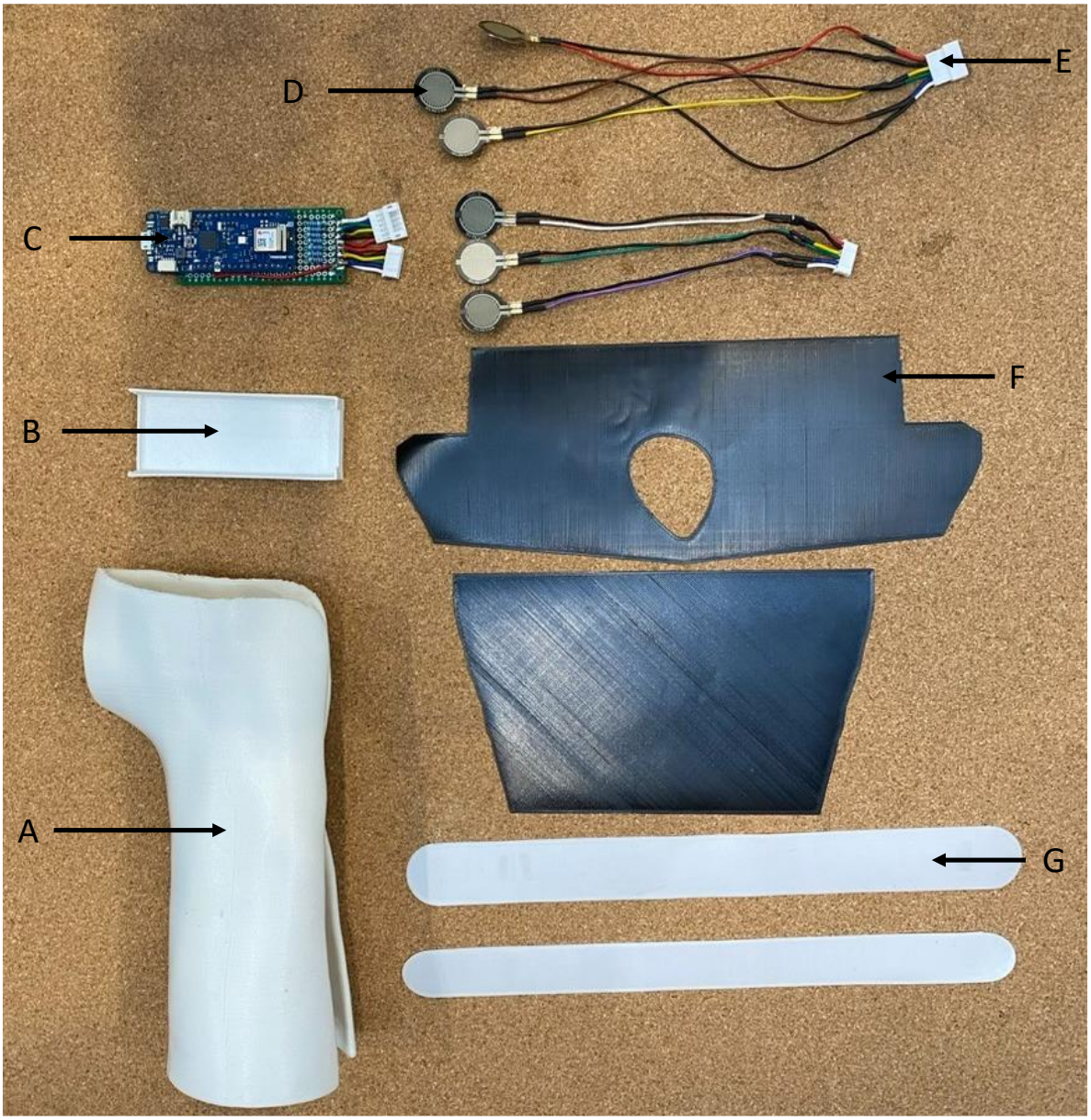

Figure 21. Representation of all the parts that consists in the 3D-printed hand brace. A) 3D-printed hand brace, B) 3D-printed Arduino case, C) Arduino MKR 1010, D) FSRs, E) Cable Connector, F) 3D-printed inner surface, G) 3D-printed straps.